POLITECNICO
MILANO 1863

Scuola di Ingegneria Civile, Ambientale e Territoriale

Master of Science in Civil Engineering for Risk Mitigation

CROSS-CORRELATION OF AMBIENT SEISMIC NOISE TO MONITOR GROUNDWATER LEVEL VARIATIONS

APPLICATION TO CRÉPIEUX-CHARMY WATER CAPTURING FIELD (FRANCE)

RELATORE: Professoressa Laura Longoni

CORRELATORI: Professore Stéphane Garambois & Christophe Voisin

Tesi di laurea di:

Marco Taruselli 838148

In collaborazione con:

Université Grenoble-Alpes,
ISTerre, Institut des Sciences de la Terre, France

ANNO ACCADEMICO 2016-2017

Table of contents

List of figures

List of tables

List of graphs

Acknowledgements

I would like to thank all the people who contributed in some way to the work described in this thesis.

First, I thank my thesis advisor Prof. Laura Longoni and the co-advisors Prof. Stephane Garambois and Christophe Voisin who provided a friendly and cooperative atmosphere at work. Their office's door was always open whenever I had questions about my research or writing. They consistently allowed this paper to be my own work, but they steered me in the right direction whenever they thought I needed it. They also allowed me to develop my project thesis at ISTerre laboratory of Grenoble, realizing my dream to work abroad.

I must equally express my very profound gratitude to my parents for providing me continuous encouragement throughout my years of study and through the process of researching and writing this thesis. This accomplishment would not have been possible without their support.

I would also like to thank my friends who made my study days less heavy.

A special thank is for my girlfriend who stuck with me during the long months of thesis's writing and she encouraged me to believe in myself and never give up.

Thank you very much!

Abstract (Italiano)

Questo lavoro presenta uno studio multidisciplinare effettuato nella metropoli di Lione (Francia), nella più estesa area Europea di captazione d'acqua potabile. Risulta fondamentale tutelare tale bacino da potenziali contaminazioni e garantire un approvvigionamento d'acqua sufficiente per far fronte ai fabbisogni giornalieri della risorsa idrica anche per scopi industriali e agricoli. A tale proposito sono stati realizzati dodici bacini di infiltrazione che permettono, da un lato la ricarica dell' acquifero, e dall'altro la creazione di una barriera idraulica atta ad evitare che potenziali inquinanti, talvolta presenti nei fiumi limitrofi, drenino nella falda sotterranea. Entrambi questi due obbiettivi comportano variazioni notevoli e molto rapide del livello di falda che possono portare al mancato rispetto della normativa che prevede di mantenere un franco insaturo di 2 m al di sotto di ogni bacino di infiltrazione. È quindi necessario, al fine di adempiere alla suddetta legge, localizzare esattamente la posizione del picco della falda acquifera e garantire un suo costante monitoraggio.

Nonostante gli studi pregressi, effettuati mediante piezometri, non è stato ancora possibile rispondere a tale necessità per via della vasta estensione superficiale dell'area (375ha). Dopo un'attenta analisi di tale problema si è quindi scelto di sperimentare il metodo della cross-correlazione del rumore sismico ambientale. Questa tecnica permette di ricostruire la risposta impulsiva del mezzo studiato, senza alcun utilizzo di sorgenti attive poiché sostituite da quelle passive che producono, per loro natura, ripetute vibrazioni sismiche nel terreno (es. fiumi, ferrovie, centrali eoliche…).

Per l'applicazione di tale metodologia sono state installate in loco dieci stazioni, provviste di geofono e di batteria esterna collegata ad un pannello solare, settate con una frequenza di campionamento pari a 250Hz. La tecnica della cross-correlazione è stata applicata sui dati raccolti da questi ricevitori per un arco temporale di circa due mesi. Questo processo ha permesso di misurare variazioni temporali di velocità sismiche (dv/v) coerenti con le variazioni di falda per una determinata banda di frequenza delle onde Rayleigh.

Il lavoro svolto ha mostrato il potenziale di tale metodologia come valido strumento di monitoraggio non distruttivo per descrivere dinamiche idrogeologiche anche in quelle aree in cui i naturali processi di riempimento delle falde acquifere sono artificialmente modificati. L'intento futuro consiste dunque nel realizzare una modellazione continua e tridimensionale dell'intera falda acquifera rispondendo così ai due quesiti inizialmente riportati.

Abstract (English)

This work presents a multidisciplinary study performed in Lyon metropole (France), in the largest European water catchment area. It is of fundamental importance to safeguard this water-field from potential contamination and to ensure a sufficient water supply to meet the daily needs of water resource for domestic, agricultural and industrial purposes. For this reason it has been decided to build twelve infiltration basins which allow, on one hand to recharge the aquifer, and on the other to create an hydraulic barrier to prevent potential pollutants, sometimes present in the neighbouring rivers, are drained into the aquifer.
Both of these objectives involve considerable and very rapid changes in the groundwater level which can exceed the unsaturated zone of two meter, mandatory by law. This zone under the basins is necessary to guarantee a sufficient filtering of the water used for the recharge of the aquifer. It is therefore essential, in order to respect the law, localize the pick of the aquifer's bulge and ensure a constant monitoring.

Even if many piezometers have been installed in the area, it is still not possible to answer to these two questions because these instruments provide a local information and it is therefore too expensive to cover the entire capturing field (375 ha). After a careful analysis of this problem, it has been decided to test the cross-correlation of ambient seismic noise method. This technique allows to reconstruct the impulse response of the medium without using active sources. In fact, the latter are replaced by the passive ones that produce, for their nature, repeated seismic vibrations in the ground (e.g. rivers, railways, wind turbines…).

In order to apply this methodology, ten seismic stations have been installed equipped with geophones and, external batteries connected to solar panels. They have been used to continuously monitor the ambient noise at a sampling frequency of 250 Hz. The cross-correlation technique has been then applied on these data, collected for a period of almost two months. This process allowed to retrieve velocity variations (dv/v) consistent with groundwater changes.

This thesis has shown the potential of this methodology as a valuable non-destructive toll to describe hydrogeological dynamics even in those areas, where the natural processes of aquifer refill are strongly modified by human activities. The future project is therefore to create a three-dimensional modelling of the entire aquifer answering to the above mentioned questions.

1. Introduction

The demographic growth, the increase in land's demand for industrial and agricultural purposes, and the risk of pollution, have led to pay greater attention on the exploitation of water resources. This need to ensure water supply throughout the year, both quantitative and qualitative, requires more accurate management of the so called *water catchment areas*. This latter can be defined as an area of land where precipitation collects into reservoirs, or drains to be stored into underground aquifers. The safeguard of these areas is necessary because the captured water often becomes drinking water for the community.
This work will move towards this purpose coupling the geophysics methods with the already exiting studies to better understand the functioning of the Crépieux-Charmy's capturing field. In particular, the main challenge of these areas is to build an overall control system that allow to continuously monitor the groundwater level. This objective has not yet been achieved even if different techniques, tests and experiments have been already carried out so far. In this perspective, taking the advantage of a well-instrumented field and a good database, it have been decided to test a passive geophysical method: *ambient seismic noise cross-correlation*. This method, that represent the core of this work, allows to monitor, and therefore interpret, continuous changes in the subsurface properties from modifications of the seismic wave propagation.

Researchers have more and more considered ambient seismic noise in Earth's subsurface imaging and monitoring in the last 15 years. They developed active imaging techniques such as seismic tomography, seismic reflection or ultrasonic imaging representing Earth's interior structure. Seismic noise investigations produced good results in volcanos, observing that small perturbations could be detected as temporal changes of seismic wave propagation properties like seismic velocity (Brenguier et al. 2008; Mordret, Shapiro, and Singh 2014; Sens-Schönfelder and Wegler 2006).
Moreover, Mainsant et al. (2012) focused on the importance of the daily cross correlation of ambient seismic noise in Pont Bourquin clayey landslide (Swiss Alps), showing that the drop of seismic velocity variations is related to pore water pressure increase and consequently to the hydrological conditions. Larose et al. (2015) proposed a review on daily noise cross-correlation technique applied as environmental seismology. They also shown that is possible to detect waves' propagation changes due to thermal, hydrological and gravitational (landslide) effects.

Thus, the Seismic noise interferometry (SNI), another name to call this technique, seems to be a good solution to continuously monitor the groundwater variations of the study area. However, it is still not proved that is possible to apply this approach in a catchment area, where the nature of the aquifer is strongly and artificially altered to satisfy the daily requirements of water. Indeed there are unnatural processes with frequent phases of

filling and draining of the infiltration basins that cause a strong and fast deformation of groundwater level (in December, within three days, there have been performed 8 cycles' charging). This strong anthropogenic influence could lead to an ineffectiveness of the interferometry method. Therefore, this work aims to validate and extend this technique to those particular cases where the ground properties, i.e. water content, change quickly in a urban environment. Whether the project will lead to positive results, means that the technique is a good starting point for development of high-resolution groundwater monitoring system. This latter will allow to build a 3D-model of the studied aquifer thanks to which it will be possible to guarantee the real effectiveness of the hydraulic barrier against the pollution and the presence of a sufficient unsaturated zone under the infiltration basins (these subjects are addressed in Chapter 2.3). In addition, it will provide invaluable data for hydrological flow modelling.

The first part of this work refers to a past thesis (Loizeau 2013) thanks to which it has been possible to give a general overview of the Crépieux-Charmy's capturing field taking into account its hydrology, geology and hydrogeology. This first section provides also a characterization of the site describing the infiltration basins with their functions and an analysis of the data collected thanks to the piezometers.
In the second part it will be shown the results of the active geophysical investigations provided and processed by students from *Polytech Grenoble* (geotechnical department).
Finally, in the third part, there will be the core of the dissertation regarding the seismological monitoring. This chapter introduces firstly the cross correlation of ambient seismic noise method giving a physical understanding of its fundamental principles. Then, the technique is applied to the seismic data recorded in the seismological stations located close to the infiltration basin 5_2. Finally the obtained seismic velocity will be correlated with groundwater level changes and the results will be discussed.

2. Site description

This chapter deals with the presentation and the characterisation of Crépieux-Charmy case study. It gives an opening overview description talking about localization, hydrology and geology. Then, it describes the capturing field from a functional point of view, providing also the piezometers data collected within the study period.

2.1. Localization

The Crépieux-Charmy site is a water catchment area located in the Lyon's agglomeration, in the Auvergne-Rhône-Alpes region (Figure 1). It located in the towns of Villeurbanne, Rillieux-la-Pape and Vaulx-en-Velin and it is crossed by different arms of the Rhone River.

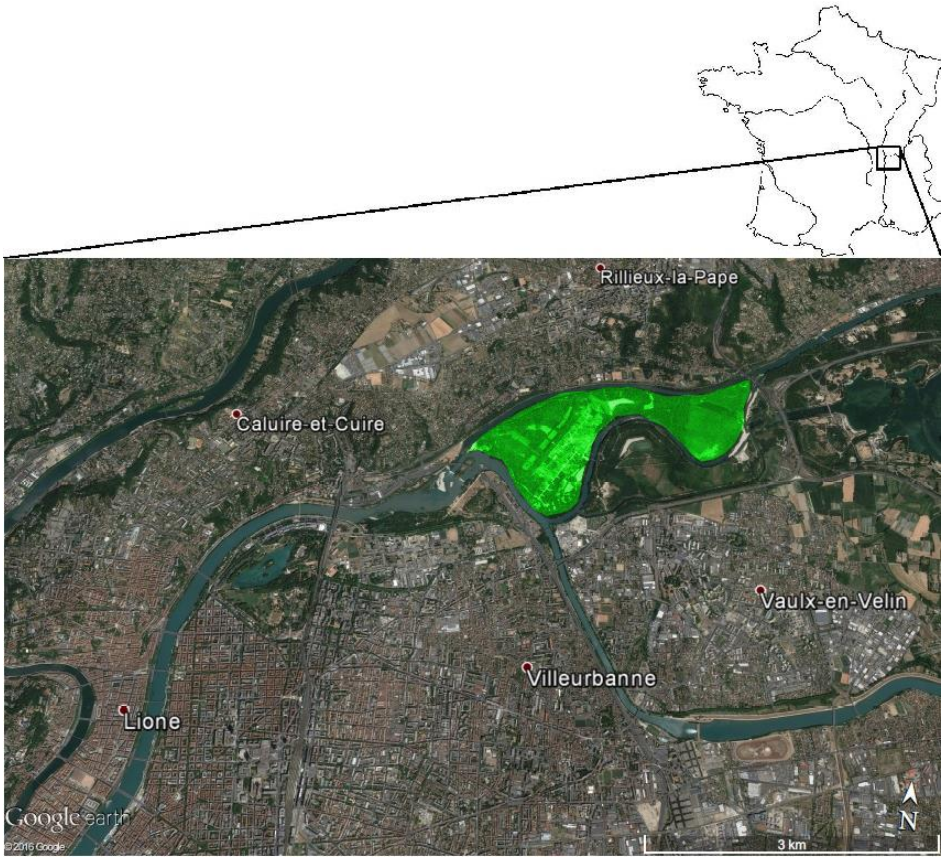

Figure 1. *Study area*

This zone corresponds to the largest water catchment field in Europe (375 hectares), which is moreover classified as a natural area of particular interest in terms of ecology and wildlife. In this context, Veolia Group has been exploiting the site since 1987 providing more than 95% of drinking water needs (150÷315 m^3/day for the 2015) for more than one million inhabitants of the Lyon's city. Even if these values could seem very high, the annual volume of drinking water supply represents only 7% of the total water

volume collected in this aquifer; the greater exploiting of water resource occurs in agriculture and industry, with the following percentage (Graph 1):

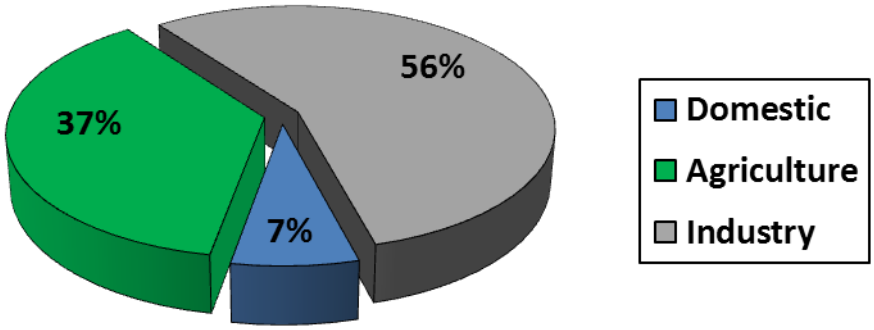

Graph 1. *Global water consumption in Crépieux-Charmy*

2.2. Hydrology and geology of the site

In the eastern part of Lyon, the fluvio-glacial deposits allow the infiltration of almost all meteoric waters. For this reason, there are no hydrographic networks other than those existing between the two arms of the Rhone: the *Miribel canal* and the *Jonage canal:*

- the first one was dug between 1848 and 1857 to facilitate navigation. With a length of about 18 km, it borders the capturing field in its northern part. The channel, at the entrance of the water catchment area, feeds two branches, the *Vieux-Rhône* and the *South canal*, then it joins the Jonage canal downstream of the site (Figure 2);
- the second one is the most southern one of the study field of Crépieux-Charmy. Commissioned in 1899, it allows a deviation of the waters of the Rhone for hydroelectric production at the Cusset dam.

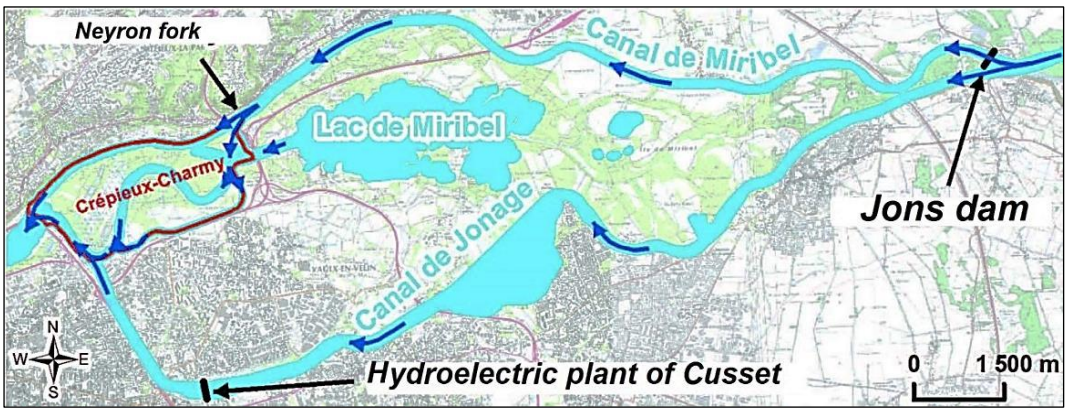

Figure 2. *Hydrology of the surrounding area*

These two channels are artificial and the area between them is called "Miribel-Jonage Island". The latter originates from a particular morphological history, strongly influenced by the anthropic activities (Appendix 1). This area gives its name to the lake located upstream the catchment: the Miribel's lake, which is mainly fed by the alluvial aquifer, and its outlet crosses the water catchment of Crépieux- Charmy joining the Jonage canal.
The hydrologic regimes of the Miribel Canal and the Jonage Canal are closely linked. Indeed, the "Jons dam", at the east part of Miribel island, is used to manage the waters of the Rhône allowing sufficient flow for the hydroelectric plant of Cusset.
The Miribel canal receives a discharge of 30÷60 m^3/s depending on the level of Lake Miribel. During the flood period, since the Jonage canal cannot contain more than 640 m^3/s, the excess flow is led to the Miribel canal. The latter's levels are completely controlled by the flow rate set at the upstream dam: for a flow rate of 30 m^3/s and 60 m^3/s, its water level is 165.45 m NGF and 165.65 m NGF, respectively.
It is important to remark that the water catchment field is located in a flood zone and therefore, during exceptional events, the flow can strongly increase flooding the study area (the most remarkable flood happened in 16 May 1983, with a water height up to 1 m). For this reason, the Vieux-Rhône channel is used, nowadays, to avoid flood in the case that the water level in Miribel canal is too high.
It can be concluded that the physical boundaries of the study water catchment area are:

- North = Mirabel canal
- South = South canal
- East = Vieux-Rhône
- West = Jonage canal

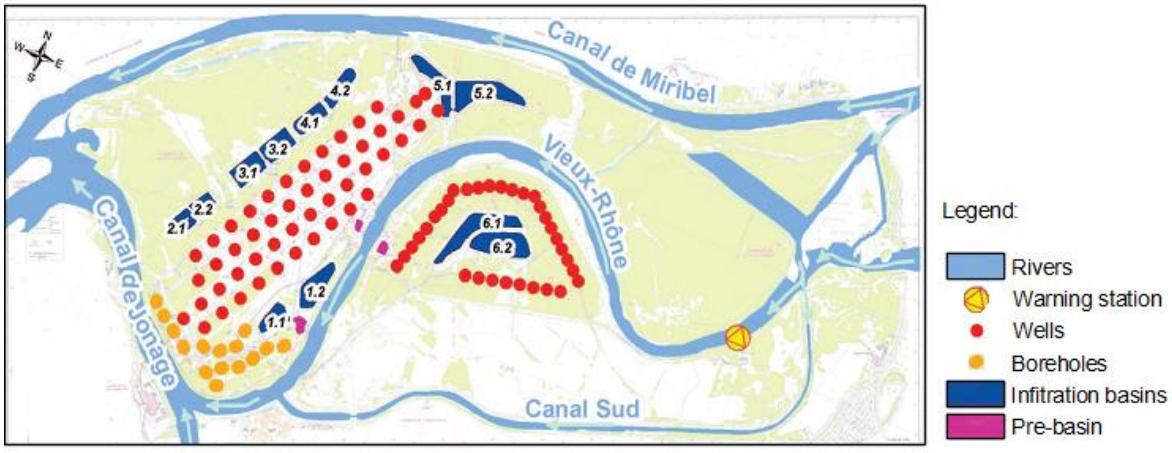

***Figure 3**: Exploitation network*

The aquifer is supported by the river/river exchanges with the Rhône, as well as by the arrivals of the fluvioglacial corridors (Decines and Meyzieu) at the Jonage canal (Figure 4). Its recharge is frequent and important with surface water, which makes it vulnerable to various pollution.

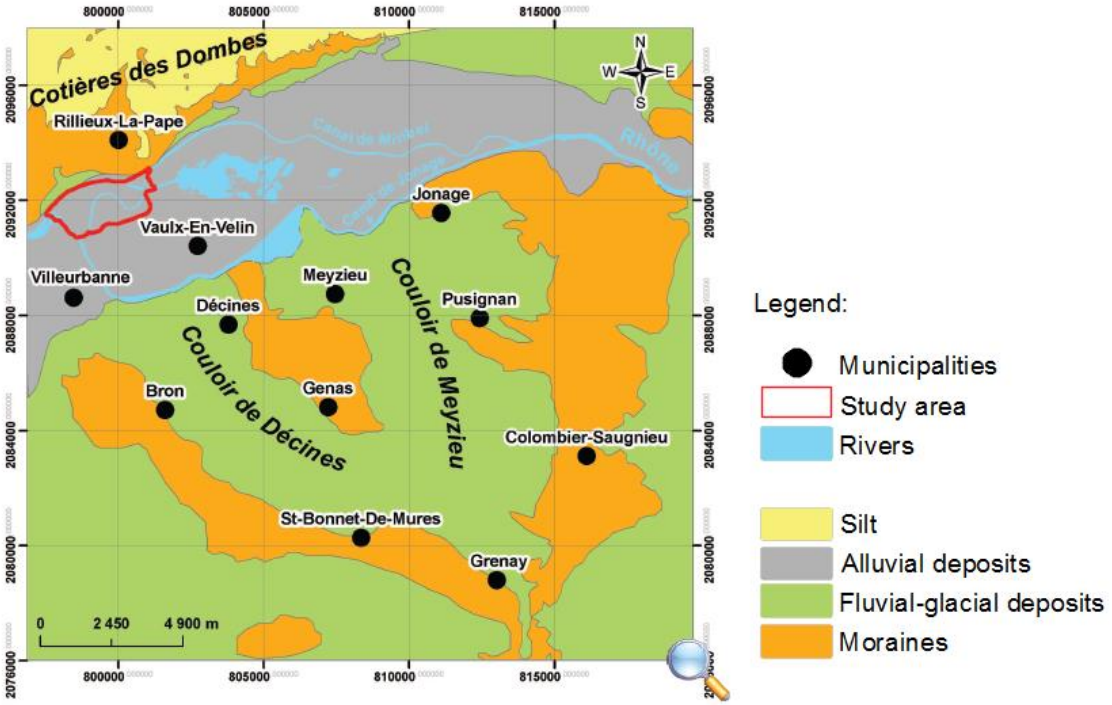

Figure 4. *Geological map*

The capturing field of Crépieux-Charmy is located between the *Bas Dauphiné* and the *Dombes*, in Miocene formations on the alluvial deposits of the Rhône. This latter is an accumulation of recent quaternary alluvium with alternating layers of fine sand, sand-gravel mixtures, clayey passages and very clean gravel-pebbles. These materials define the permeability of the aquifer, generally between 1.10^{-3} m/s and 5.10^{-2} m/s.

Soil	*Permeability Coefficient, k (cm/sec)*	*Relative Permeability*
Coarse gravel	Exceeds 10^{-1}	High
Sand, clean	10^{-1} to 10^{-3}	Medium
Sand, dirty	10^{-3} to 10^{-5}	Low
Silt	10^{-5} to 10^{-7}	Very low
Clay	Less than 10^{-7}	Impervious

Table 1. *Permeability coefficient k (cm/s)*

More information have been collected during the building of piezometers. They make it possible to know the total depth of each layer as well as the lithology encountered. The following figure is a summary of the geological sections observed in the study area.

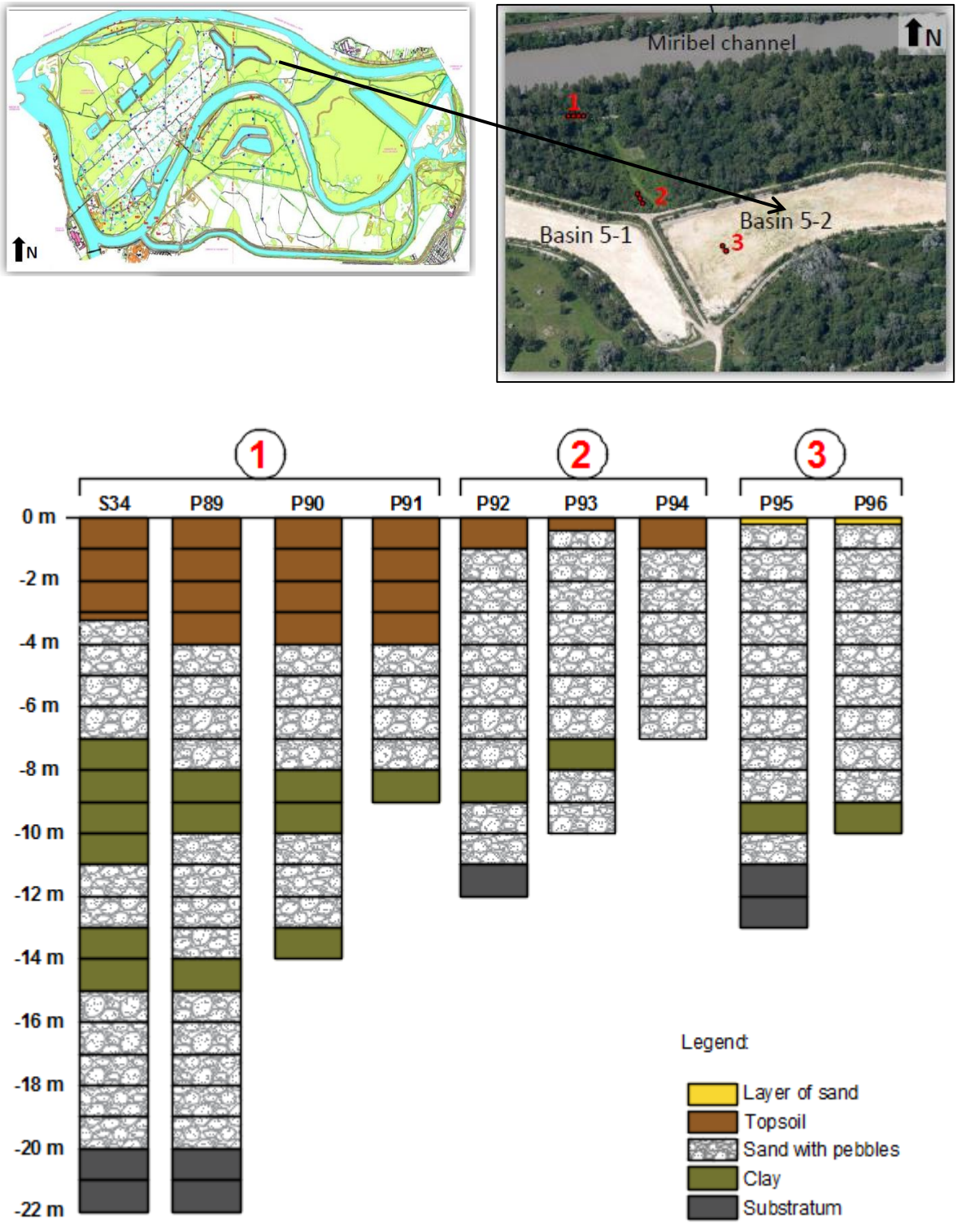

Figure 5. *Geological sections*

2.3. Management of the water resource

The catchment field counts 114 wells that participate in the pumping of the water resource. These structures have been designed to provide a daily flow of 600'000 m^3/d. The average daily withdrawals, over the last ten years, are around 250'000 m^3/d with peaks up to 420000 m^3/d (June 2002 or June 2003). The number of active pumping wells vary in a day, depending of the availability of the structure due to the frequent maintenance. Furthermore, the withdrawal of water has a day/night operation according to time constraints of the energy supplier. Thus, during off-peak hours (night) the pumping flows are very high in order to fill the reservoirs and, during the day, the pumping flows are much lower. This discontinuity in the pumping produces fast changes of the groundwater.

In order to guarantee a good water quality, two warning stations (physicochemical measurement stations) are used to detect any potential pollution of the surface waters. One, located inside the capturing field (Figure 3), continuously analyses the quality of the water and in case of non-conformity, the water supplies to the basins is immediately cut off. The other one, located 14 km upstream the study area, allow to give a pre-alert in the case of pollution. Tracing tests carried out in 1999 made it possible to determine the transfer times of the arrival of a pollutant between the two warning stations. The transfer was estimated at 2 h 40 via the Miribel canal for flows between 280÷305 m^3/s.

In addition to these monitoring stations, water sampling is periodically carried out on all the pumping wells to have a constant monitoring of the water quality. If the analysis reveal a presence of pollutant in the aquifer, the supply of drinkable water is guarantee by a treatment system that purify the Miribel's lake water.

Furthermore, to prevent the proliferation of bacteria in the network, the chlorination of the pipelines and pumps is carried out.

2.3.1. Aquifer recharge method: Infiltration basins

In the natural process, the recharge of the water table is effected by meteoric waters (rain and snow melt), by infiltrations of watercourses and by the arrivals of the fluvioglacial corridors. When this is not enough, the artificial groundwater recharge can provide a truly effective solution. This method is an anthropogenic process that consists in increasing, by artificial means, the amount of water that enters to the groundwater reservoir. In 1989 this approach was applied in Crépieux-Charmy with the design and construction of 12 infiltration basins with a maximum recharge rate of 389'730 m^3/day. This decision was taken after a very dry season, when the low flow of the Rhône brought the capturing field to the limit of its exploitability.

The aim of the technique is to "inject" water into the soil that will percolate to the water table. When the incoming volumes are greater than the volumes that can be locally

evacuated, a rise in the groundwater occurs. This process create a parabolic shape of the water table with its maximum localized under the surface of infiltration (Figure 6). The aquifer must have suitable physical characteristics in order to limit the maximum of the water table and thus preserves an unsaturated zone under the basin (at least 2m).

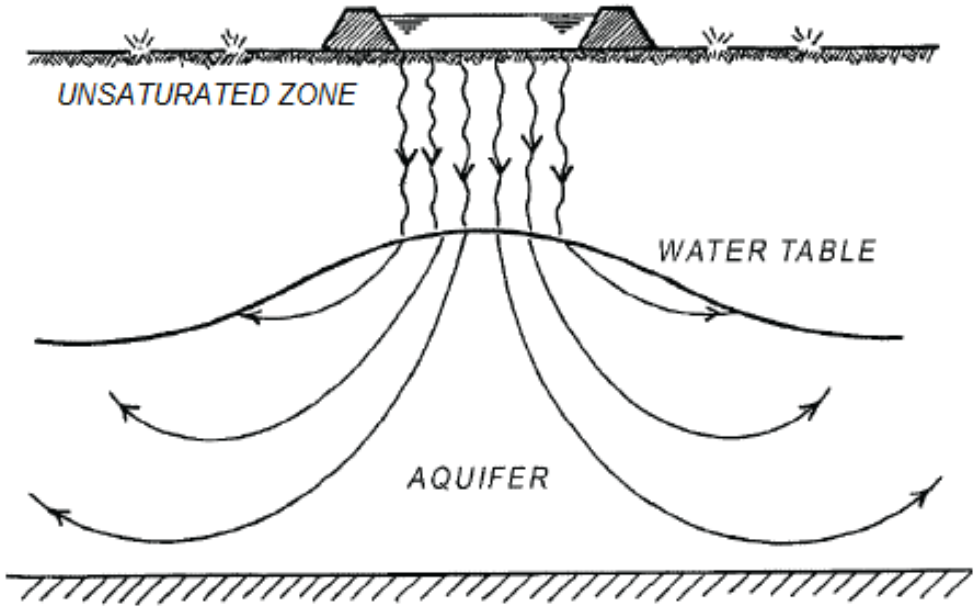

Figure 6. *Formation of the bulge under the infiltration basin due to the recharge procedures of the aquifer.*

Infiltrated volumes depend both on the area available for infiltration and on physical characteristics of the layers under the basin. These latter must guarantee a good purification of the water used for the recharge and a sufficiently short time period for the percolation in the aquifer. In the study case the recharge volume has two main goals:

- First at all it allows to support the decrease of water levels generated by the withdrawals of the pumping site;
- Secondly, but not least, makes it possible to generate, by inversion of the gradients, changes in flow directions in the aquifer to protect it against river's pollution. This is possible thanks to the parabolic shape of the water table (Figure 6), which generates an hydraulic barrier. However, for safety reasons, any pollution of the Rhône's water and any flood warning must lead to the immediate cessation of the water supply to the basins.

2.3.2. Functioning and design of the hydraulic barrier

The risks of pollution of the Rhône, upstream the Crépieux-Charmy field, is linked to the large number of domestic and industrial discharges. Indeed, nearby the study area, there are industrial factories and communication routes (railway or road) that can be sources of pollution. Most of the waste water do not undergo any treatment of purification before it is transferred into the Rhône. The dynamic protection of the aquifer would consist in creating an hydraulic barrier by injection of water between the Rhône and the pumping wells thanks to the infiltration basins. The objective of the hydraulic barrier consists in reversing flows in the groundwater to repel the pollution that would have infiltrated through the banks of the river.

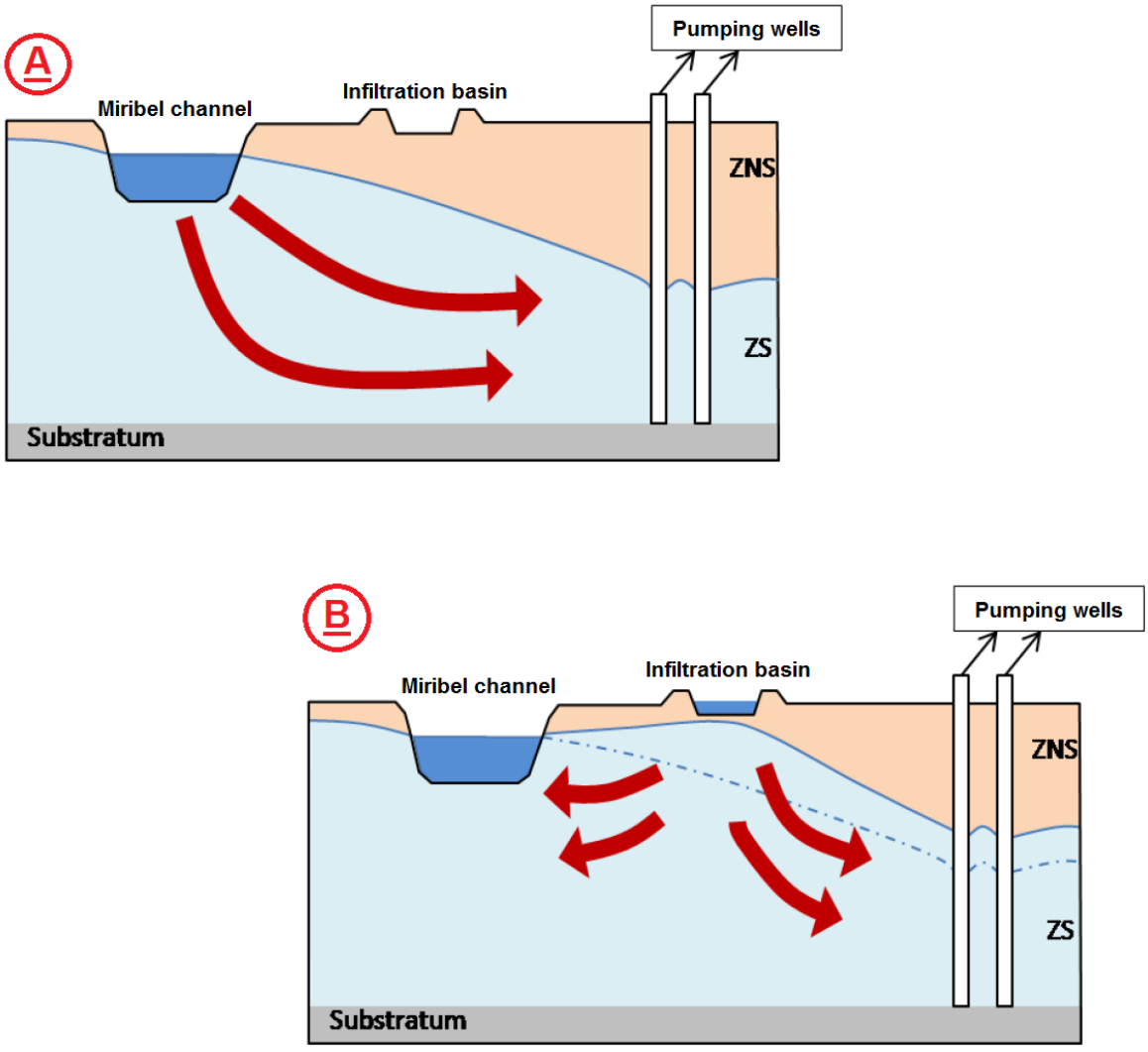

Figure 7. *Principle of operation of the hydraulic barrier: A= Empty basin; B=Full basin*

In 1989, following various numerical simulations of the aquifer's response, the configuration considered to be more efficient for the purpose, consists in a series of 12 infiltration basins (Figure 8). With this solution the total area available for infiltration is about 147000 m^2 for the entire catchment area.

Figure 8. *Map of the catchment area with the location of the basins*

The infiltration basins were dug in the fluvial-alluvial deposits of the Rhône, considering zones of high hydraulic conductivities. The layers of clay, less permeable than sand, gravel and silt, have been removed where possible.

The basins have a defined depths in order to maintain an unsaturated zone of 2 m between the bottom of the basin and the maximum level of the groundwater. The maintenance of this zone is mandatory by law and necessary for a good water purification. According to the initial design, the monitoring of this thickness is controlled by the piezometers that provide a localized measure. For this reason it is not yet proven that the obtained measures referred to the highest point of the bulge, and therefore the 2 m of unsaturated layer is not yet guarantee.

The infiltration basins can be recharged by river diversions or thanks to a system of water pipes. The water, for the recharge of the basin located in the study area (basin 5_2), is derived directly from the Rhône and collected in a pre-basin. The latter allows to decant river's water in order to prevent that pollution and sediments will be brought in the infiltration basin.

Figure 9. *Pre-basin*

The water of the pre-basin is then pumped to the infiltration basin by a canalisation as shown in Figure 10. In order to be simultaneously able to carry out maintenance operations and allowing the recharging of the aquifer, the infiltration surfaces were divided into pairs of basins that can work independently.

Figure 10. *Pipeline to bring pre-basin's water in the infiltration basin*

The injected water can cause progressive clogging in the bottom of the basins. In order to maintain good infiltration capacity, the basins are covered, for a thickness of 30 cm, with a "filter" layer of sand. To make the ordinary maintenance less problematic, the granulometry of this layer is dimensioned to prevent its transit in the alluvium deposit.

Figure 11. *Section of the infiltration basins. The "filter" layer is clearly identifiable above the alluvial layers on the infiltration basins*

2.4. Piezometer data

This paragraph shows the piezometers' data provided by the monitoring center of Veolia's company. They referred to the surrounding area of Basin 5_2 where the seismological stations have been installed for the monitoring of the groundwater level. This zone, located on the north side of the capturing field (Figure 12), is equipped with 7 piezometers that continuously measure the aquifer level. Their position should allow to broadly reconstruct the bulge generated under the basin during the recharge processes. However, as already said, the piezometers provide a local measure and thus are not enough to localize exactly the bulge and its maximum peak. This limitation could be overcome with passive seismic interferometry depending on this preliminary tests.

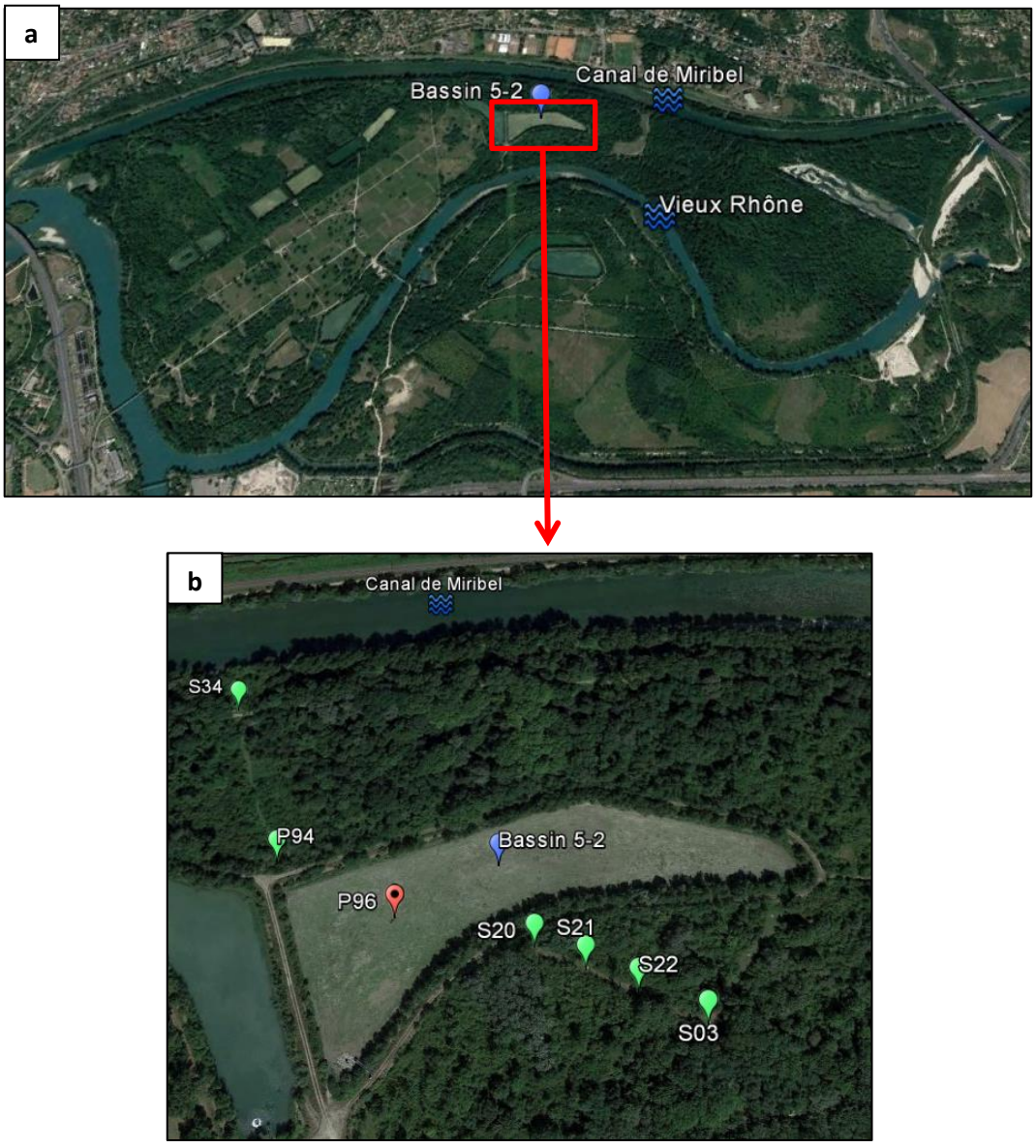

Figure 12. a) *Capturing field of Crépieux-Charmy;*
b) *Detailed of the studied basin and piezometers' position.*

The following graph refers to the period between 30th November 2016 and 30th December 2016. The upper black curve represents the water level measured inside the infiltration basins 5-2. The others refer to the data collected in various piezometers. In particular, those with shades of green denote the piezometers located at south of the infiltration basin; the shades of blue those in the north part. Finally, the red one, represent the piezometer installed inside the basin; it is important to note that the groundwater level recorded on it is the closest one to the surface.

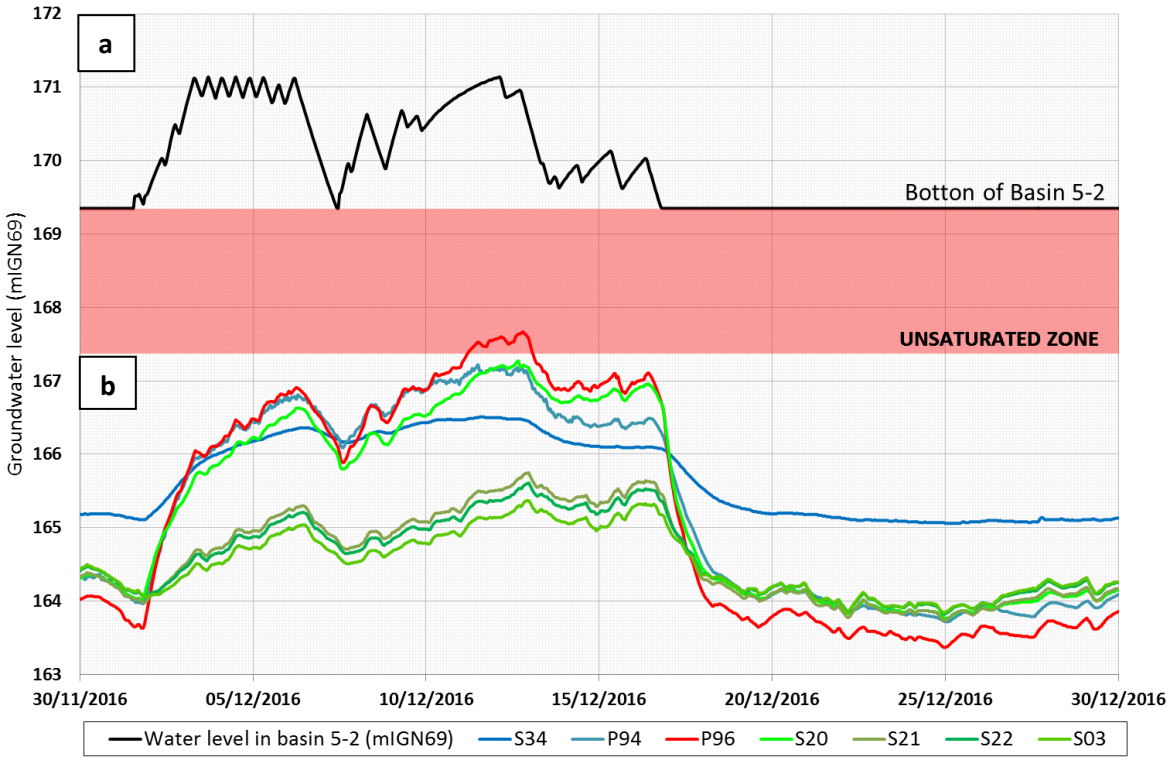

Graph 2. a) *Water level inside the infiltration basin 5-2.* ***b)****Groundwater level evolution*

From the black curve it is possible to see the basin refill cycles occurred within December. As expected, the ground water level of the aquifer increase due to this processes and then it undergo a significant decay when the recharge is stopped. It is possible to see this behaviour in all the plotted data with different intensity. Only the piezometer S34 shows a smoother trend, but it is probably due to the fact that it is located close to the Miribel canal and therefore it is influenced by the infiltration from the riverbanks. Thus, this piezometer will not be compared with the computed velocity changes.

As can be seen from the graph, the aquifer level, measured in piezometer P96, exceeds the limit imposed by the unsaturated zone for a period of almost 2 days (46h). Due to the fact that the bulge has not yet been identified with certainty, it is reasonable to suspect that the limit of 2 meters is violated for a longer period.

3. Geophysics

The thesis' project concerns the region which includes the infiltration basin number 5_2. However, the geophysical results, provided from the *Polytech Grenoble*, refer only to the south part of the basin (Figure 13). This choice has been made according to two main reasons: first at all because it is supposed that the aquifer's bulge is located below this area; the second reason is the high number of piezometers, which huge amount of data can be used to confirm the geophysical results.

The objectives of geophysical investigations are multiple: the main goal is to determine the groundwater level and the substratum depth in the shown area. Secondly, but not least, the aim is to detect the less permeable zone and to evaluate the water content. In order to increase the accuracy of these measurements different techniques will be used.

For the presented case, study has been using four methods whose outcomes are deliberately similar to confirm the observations thanks to the cross-checks of data. Thus, in the following paragraphs, after a brief theoretical description of each geophysical method, the main results will be shown (Bonneton, Jacquemard, and Taxil 2016).

3.1. Geophysical investigations

The active geophysical measurements chosen for the capturing field involve the realization of a seismic and electrical tomography, as well as Ground Penetrating Radar investigations. The coupling of these methods will allow to construct an image of the subsoil to better characterize the groundwater level and the unsaturated zone.

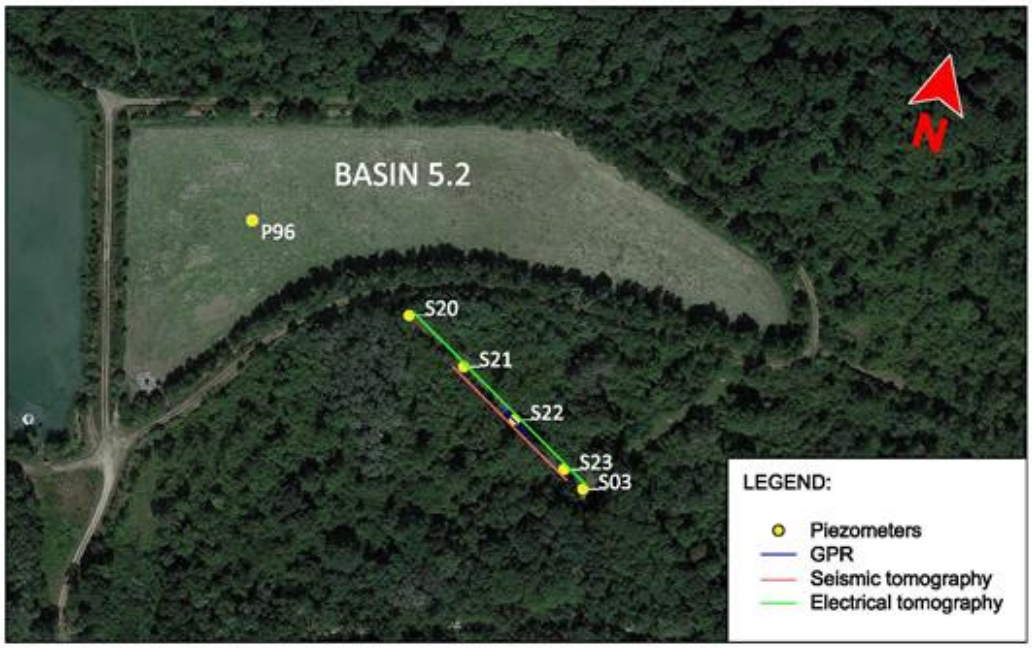

***Figure 13**. Location of geophysical investigations*

3.1.1. Seismic tomography

It is a technique to measure and display the three-dimensional distribution of velocity (or reflectivity) of a volume of the Earth by using numerous sources and receivers located on the surface. In tomography the substratum is divided into cells, each having a certain velocity. These are obtained through an inverse problem in which travel time data are compared with an initial model and the model is modified until the best fit is reached between the model prediction and observed data (Seismic Tomography 2017). The final result is a velocity distribution, which has to be interpreted. With regard to the presence of water, it is known that the velocity of the P-waves (primary or pressure waves, Vp) increase in saturated soil (> 1500 m/s) whereas the S-waves (secondary or shear waves Vs) are not so sensitive to the presence of the water table. This technique can thus be used to do a first check of the groundwater level.
In order to reach the substratum, and so to cover a depth of almost 15m, a profile of 24 geophones spaced 2.5 m apart has been installed.

3.1.2. Electrical Resistivity Tomography

The resistivity technique is a useful method for characterising the sub-surface materials in terms of their electrical properties. Variations in electrical resistivity (or conductivity) typically correlate with variations in lithology, water saturation, porosity and permeability, geological structure and groundwater (Electrical Resistivity Tomography (ERT) n.d.). The Electrical tomography can thus identify the ground's structure saw in the piezometers and the roof of the water table thanks to the different resistivity. The acquisition of resistivity data involves the injection of current into the ground via a pair of electrodes and then the resulting potential field is measured by a corresponding pair of potential electrodes (Electrical Resistivity Tomography (ERT) n.d.). Finally, iterative tomographic inversion of apparent resistivity data, yields a two-dimensional model of specific resistivity which represents the true resistivity distribution of the subsurface section (Hilbich et al. 2008). The field set-up requires the deployment of an array of regularly spaced electrodes and, since it would be necessary to investigate up to 14 meters (substratum should be at -12 m), they have been spaced 1,5m each other over a distance of 84 meters (Investigation Depth = AB / 6 = 84/6 = 14 meters).

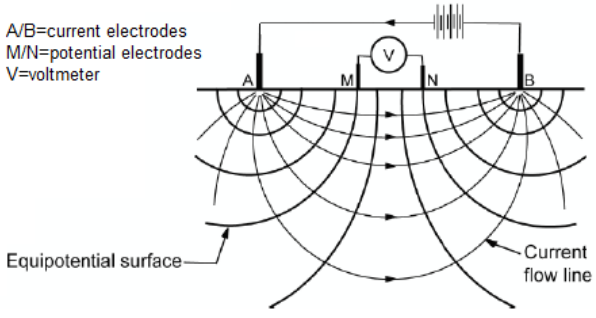

Figure 14. *Electrical resistivity measurement principle*

3.1.3. Ground penetrating radar

This technique is used to explore the subsoil sending electromagnetic waves; when there are changing in material properties, part of the wave is reflected by interfaces and recorded by the antenna. The GPR methods used for the project are the common mid point (CMP) and the Constant-Offset profiling.

In the **common mid point (CMP)** the general idea is to acquire a serie of traces (gather) which reflect from the same common mid-point ("Electrical Resistivity Tomography (ERT)"). This latter can be approximated in the vertical line in the mid-way between the emitter and the receiver. The analysis of the time-distance relation, for all the observed reflectors, allows to estimate the velocity variations according to the depth. Thus, the aim of CMP experiments is basically the collection of data suitable for velocity analysis. It must be noted that EM velocity is strongly dependent on water content.

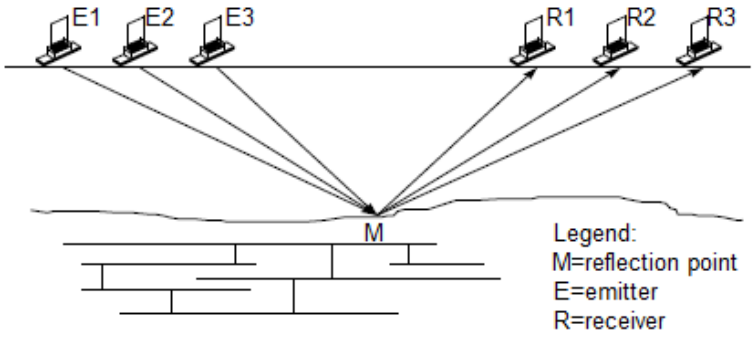

Figure 15. *Schematic representation of a common mid-point experiment*

The second method is named **reflection method** and the emitter and the receiver are used to collect near-vertical reflections as shown in figure 16. The aim of this type of survey is the production of high resolution sections that depict the reflection boundaries, and so the discontinuities of the medium, and, in this case, also the permeability's changes.

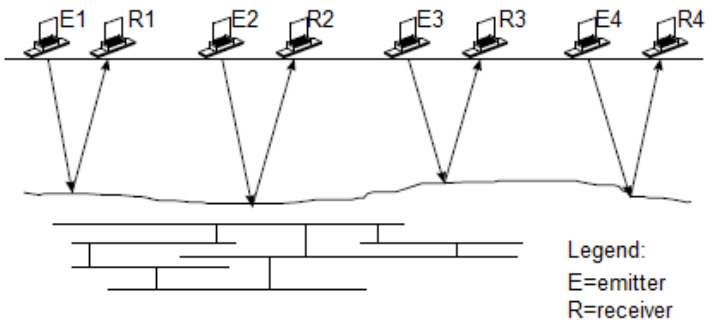

Figure 16. *Schematic representation of a GPR reflection survey*

3.2. Results

Here below it shown the result of each technique and a global synthesis of all the elements that allow to construct an interpretation of the site.

3.2.1. CMP

The CMP was performed using 100 MHz antennas close to piezometer S22. Moving the source and the antenna for a constant step of 20 cm, it has been cover a distance of 8m. In the following pictures the results of CMP test:

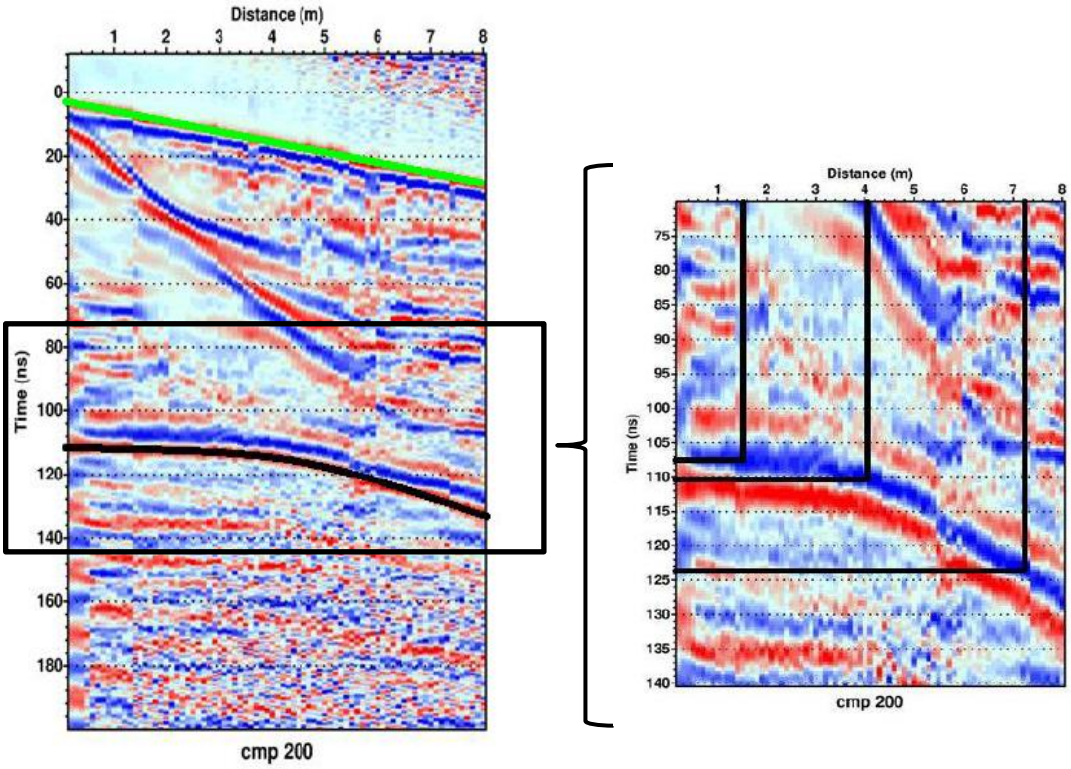

Distance [m]	Time [ns]	Distance^2 [m]^2	Time^2 [ns]^2	Velocity [cm/ns]
1,5	107,5	2,25	11556,25	**11,22**
4,1	110,5	16,81	12210,25	
7,2	124	51,84	15376	

Figure 17. *CMP profile and computed velocity*

As expected, the computed direct wave in the air (green line with a linear trend) has a value of velocity equal to 27.61 cm/ns, almost equal to the speed of light (30 cm/ns). Instead, analysing the hyperbola has been obtained a speed of 11.22 cm/ns which allows to determine various parameters with the relationship between the dielectric permeability and water content. In fact, in the study case has been obtained that the water content is about 10%, with the reflector (the groundwater table) at 5.60 m. The ground above the aquifer is almost dry, which will potentially lead to an high electrical resistivity.

3.2.2. Reflection

This method was performed along a profile where the CMP was located, with shielded 250 MHz antennas. The electromagnetic pulses are transmitted at fixed time interval and, travelling inside the material, part of them are reflected by the reflectors. Thanks to this it is possible to determine the different horizontal layers as well as the evolution of the aquifer.

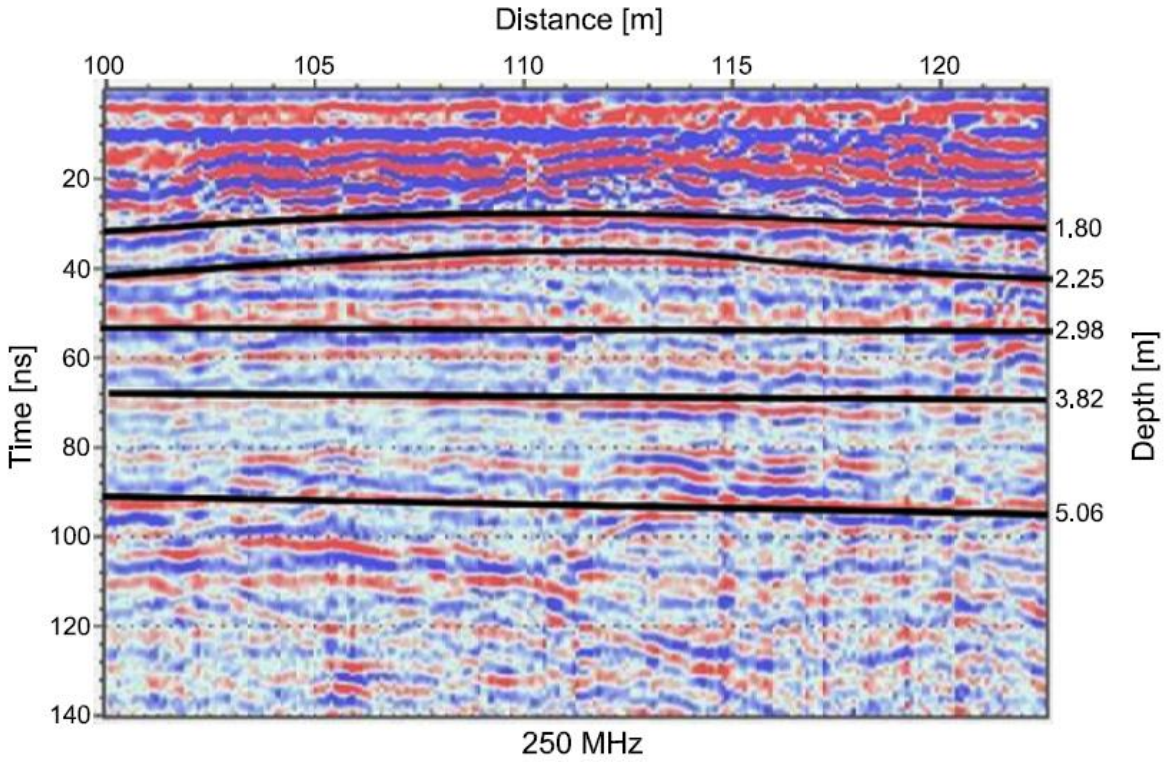

Figure 18. *GPR profile*

The six identified layers are very linear, this is probably due to the sedimentary deposits of the Rhône. On the other hand their thicknesses are not constant, ranging from 0.5m and 1 m (Figure 18). The reflectivity of these layers are different due to the fact that the materials' grains size vary depending on the depth. This leads to the conclusion that the activity of the Rhône changed along the years generating a variable sedimentation.

3.2.3. Seismic tomography

For seismic tomography 24 geophones spaced every 3m (total length of 72m) have been disposed on the ground and an hammer has been used as a source.

P-waves

The analysis of P-wave allows to perform the tomography shown in the figure below. It is possible to see immediately the horizontal stratigraphy under the interested area and, thanks to the obtained velocities, a first hypothesis concerning the composition of the ground has been carried out. The first meters have velocities between 300-600 m/s and may correspond to a layer of topsoil composed by unsaturated sand and gravel. Going deep the compaction of the materials seems to increase according to the velocity changes. In fact, around 6 m depth, the speed is of the order of 1500 m/s, which seems to indicate the presence of the water table. The speed continues to increase gradually in the next few meters, still indicating the presence of coarse and saturated materials. At about -10m there is a change in lithology which indicates the beginning of a clay layer. If the impermeable substratum is composed by clay, as shown by the boreholes, it is not possible to discern it clearly from the aquifer because they have similar velocities. Moreover it appears at the limit of investigation's depth of the seismic profile.

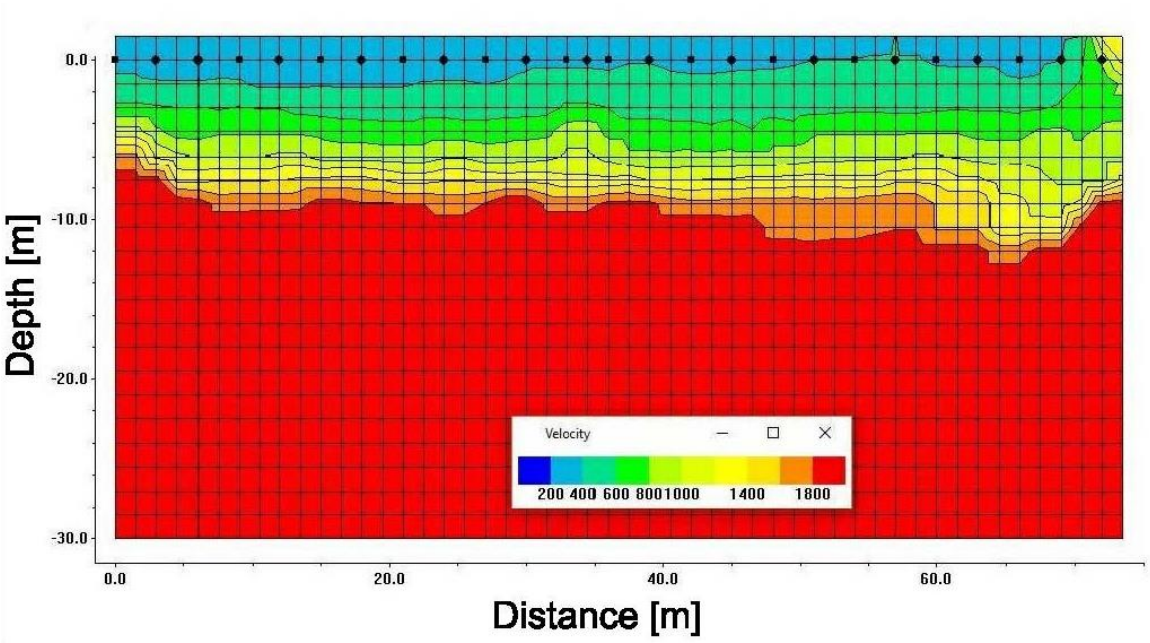

Figure 19. *Seismic tomography of P-waves*

S-waves

The study of S waves returns the compactness of the geological layers previously identified, but especially it provides the level of "Bedrock". This latter is formed by grey

clay and it should be characterized by a velocity propagation of 750-1000 m/s. The obtained result, shown in the figure below, has been reached after ten iterations with a final RMS of 4.5%. It can be observed a progressive increase in propagation velocities depending on the depth, which means an increase in compactness. In particular, at -12m depth there is a significant contrast which is probably associate with the compact grey clay ("Bedrock"). There is not signature of the water table, as expected from S-waves images.

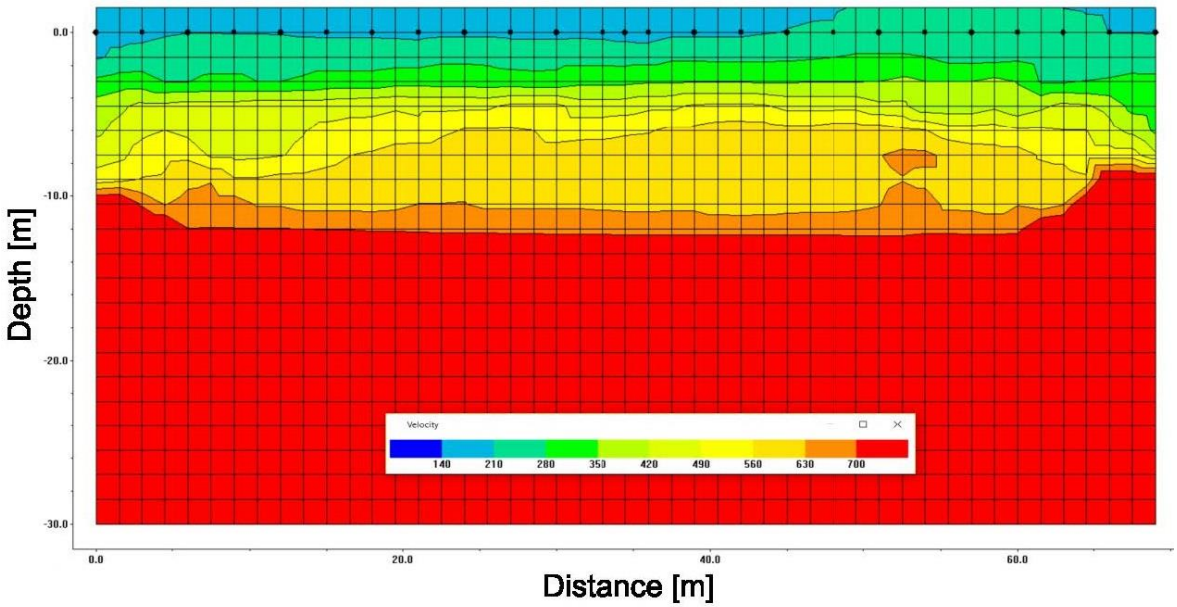

Figure 20. *Seismic tomography of S-waves*

3.2.4. Electric Resistivity Tomography

The electrical resistivity tomography measurements, performed with 72 electrodes, were carried out with two configurations: the Wenner and the Dipole-Dipole. The first one has a high sensitivity in recognizing vertical variations of resistivity, therefore it allows to distinguish very thoroughly the vertical structures. With this configuration 1111 measurement points have been performed in a single “pseudo-section”.

The second one is more sensitive to lateral variations and it has a reduced investigation depth.

The objective of the inversion is to create a resistivity model that correspond, as precisely as possible, to the ground data. The consistency of the obtained models are based on two main indicators: RMS and Chi². The RMS is a function of inversion’s quality and it is a measure of the difference between values predicted by the model and the field measurements. The Chi² is used to indicate initially the consistency of the model (Chi² must be less than 1).

Wenner configuration

The model obtained, with the Wenner mode, shows in the central part the main horizontal discontinuities. Close to the surface there is weak resistivity (100-300 Ω·m) which correspond to the topsoil. Between 2 and 8 meters there is the layer with the highest resistivity and it would correspond to a more dry and coarse materials and therefore to the unsaturated zone. This is due in particular to the permeability of sands and gravels that directly transfer water to the acquifer. The clay layer, with a very low resistivity (30-50 ohm.m), clearly marks the deepest part detected. Between this latter and the unsaturated area, at a depth of around 10 meters, an interface appears clearly indicating the presence of water and fine materials. This will be better characterized with the Dipole-Dipole configuration.

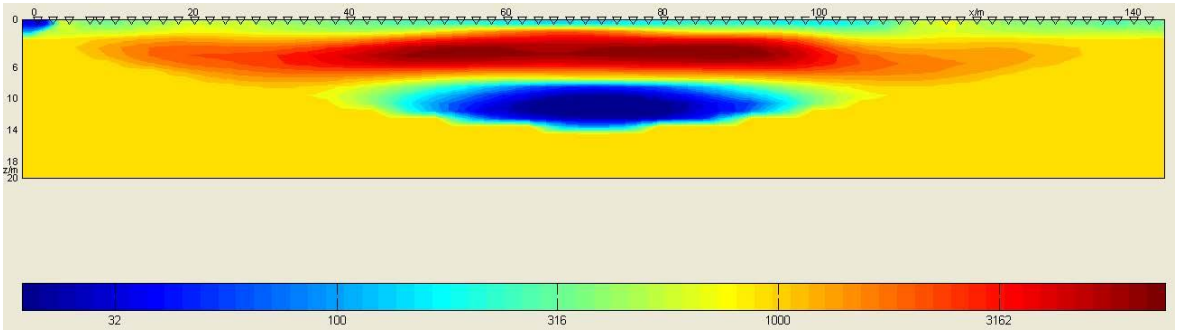

Figure 21. *Electrical tomography_Wenner configuration*

Dipole – Dipole configuration

The Dipole-Dipole configuration should provide better horizontal resolution. From the obtained result is possible to distinguish three interfaces. The first interface marks the passage between the superficial slightly moist zone and the permeable alluvial layer. The second one, at -8 meters, can be associated with the water table because there is a progressive decrease of the resistivity. The last interface, at a depth of around 11-12 meters, corresponds to the bottom grey clays characterized by a high conductivity. In general, the highlighted elements have horizontal configurations.

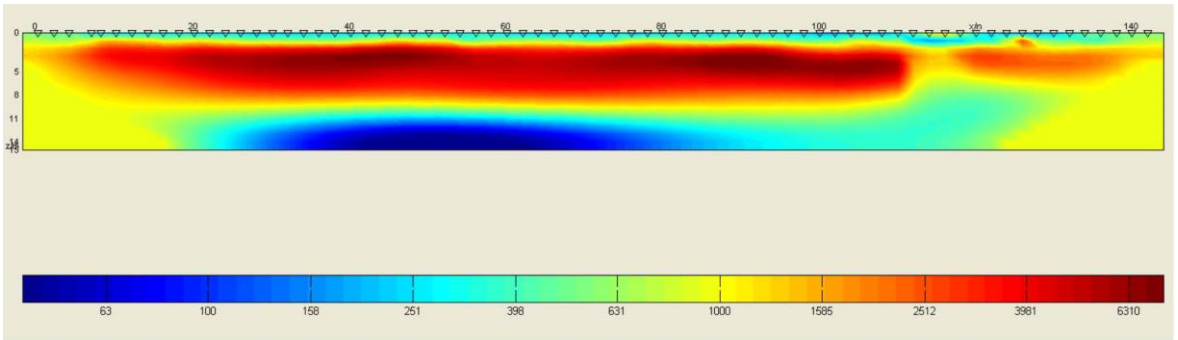

Figure 22. *Electrical tomography_DD configuration*

3.3. Discussion

The previous geophysical results have been compared with the geological section obtained during the drilling of the piezometer S22. The borehole, below the topsoil, reveals coarse material over a large thickness up to 12 m; this have a high permeability which explains the reason why the water goes quickly deep. Then there is a layer of clay, very impermeable, which is clearly recognized also in the geophysical tests.

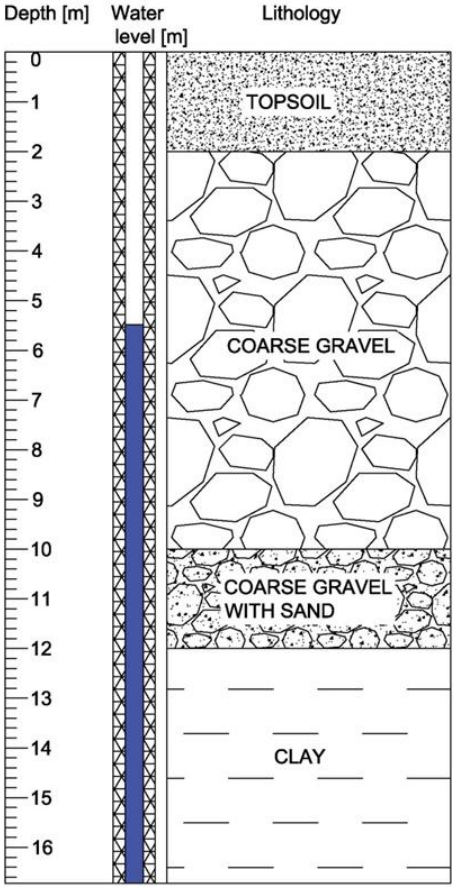

Figure 23. *Borehole*

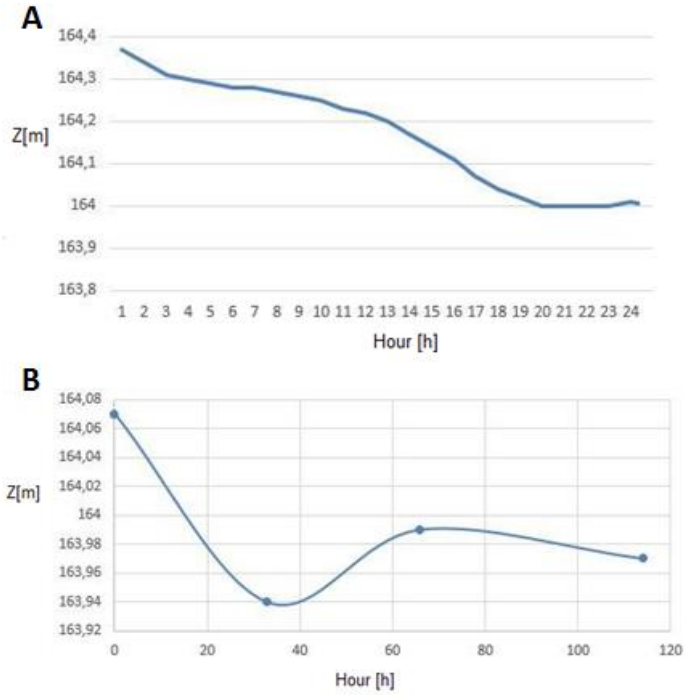

Graph 3. ***A****=water evolution during the hour of the survey's day;* ***B****=water variation along geophysical survey.*

Thanks to the piezometer data it can be observed that the groundwater level is between 5 and 6 m but it has decreased by 40 cm, which may be due to the pumping carried out on site for the water supply of Lyon. At the same time, the water level has a fluctuation of about ten centimetres along the length of the study profile. This will be difficult to detect due to the resolution of the profiles.

All the above geophysical methods give the horizontal configuration of the ground providing just a 1D model. However, combining the results with the piezometers data, it is possible to obtain an interpretation of the subsoil in the study case.

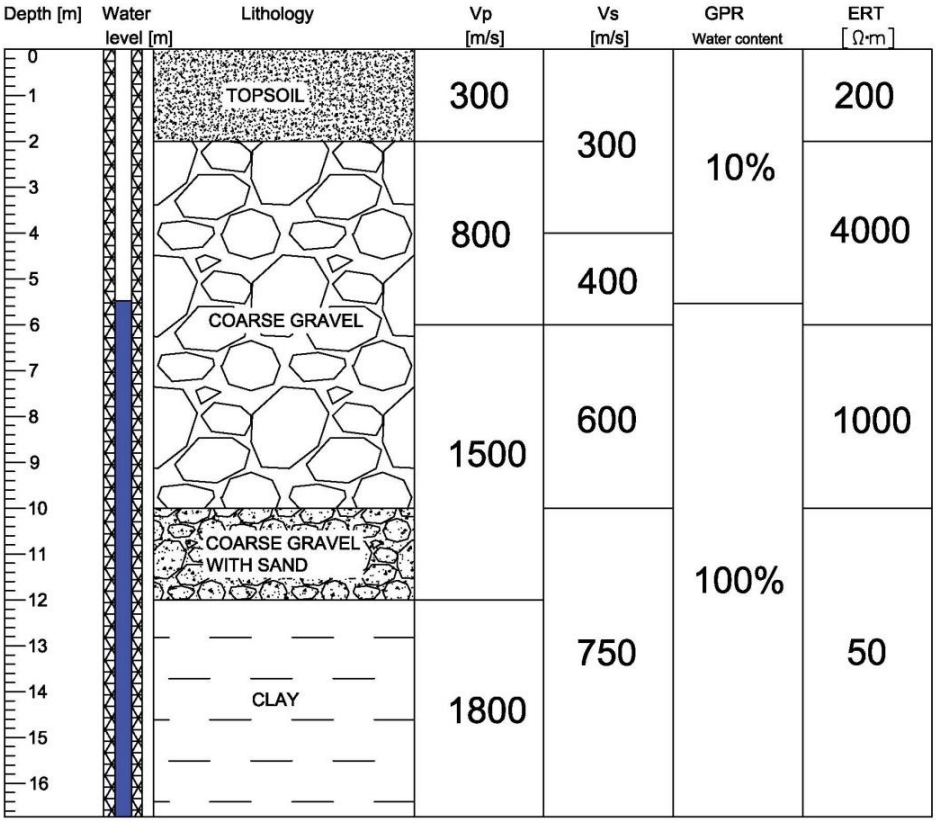

Table 2. *Summary of the data collected by treatment*

The result of the GPR CMP are the most accurate for the detection of the water table; in fact it provides a value of groundwater level around 5.6 m.

The seismic and electrical tomography were compared to support the hypothesis. A saturated zone has been observed between 6 and 10m which would correspond to the bottom of the sandy gravel layer, before gradually finding the impermeable clays. The aquifer is characterized by waves Vp = 1500m/s and resistivity considerably lower than the dry gravel (between 2 and 6m). The water content of this upper layer is verified by the GPR which gives a content of the order of 10% (the sandy gravel layer is very permeable). It can thus be proved that the top of the aquifer is located at about 6m depth by relying on geophysical prospecting. This hypothesis is verified by the piezometers located along the profile that provide a depth between 5 and 6 m, with variations during the day. The electrical tomography proved to be of poor quality for this environment and it could not provide precise information. Used alone in the field, it would not have been possible to make a clear interpretation of the data. Therefore it is important to couple several techniques to increase the precision of the hypotheses. Note that in this case the working space and time were quite restricted, which could lead to magnetic noise, especially during the radar survey (electrical tests and GPR in parallel).

4. Seismology

This chapter represents the core of this work because it deals with the cross correlation of ambient seismic noise method. Particularly, after an introduction illustrating the reasons which led to the use of this technique, and some past researches examples, the physical understanding of the method is presented. Then, the following part is about the method's application to Crépieux-Charmy case study with a final section about results' interpretation.

4.1. Introduction

Seismology has long been considered to be the primary source of information on the structure of the Earth, and deep Earth studies have raised a broad scientific interest (Astiz, Earle, and Shearer, 1996). Based on these observations, and thanks to recent progresses in hardware technology and computational power, seismologists are trying to develop new techniques that allow to monitor continuously over time the subsurface. However, this is not an easily reachable goal because it requires a reproducible seismic signal which propagates constantly into the ground (Larose et al. 2015). Thus, the major handicap which hinders continuous monitoring in the field is the requirement of repeatable sources.

This latter used to be exclusively achievable with active sources (explosives, hammer blows, etc.) or with the seismology methods based on earthquakes (Ratdomopurbo and Poupinet, 1995). Unfortunately, the first solution is economically too expensive and the studied areas are not always easily accessible; the second one has instead a limited resolution in those geologically active areas and, the sporadic occurrence of the earthquakes, make not possible to build a permanent and reliable monitoring system.

In order to overcome these problems, the researchers tried to work on the wave-field that it does not depend on earthquake occurrence and can be recorded at any time and any location: the ambient seismic noise. This latter can be defined as the ground motion which is recorded in the absence of an identifiable active source of seismic energy (IASPEI/IAVCEI Joint Commission on Volcano Seismology - Tutorial 6 - Seismic Noise Interferometry. Retrieved from http://volc_seis_commission.leeds.ac.uk/indexa63d.html). Examples of these passive sources are everywhere and consequently it can be assumed to be in a diffuse field. The ambient seismic noises can be divided into microseisms (low frequency waves < 1 Hz) due to natural causes (mainly ocean waves (0.1 – 0.3 Hz)) and microtremors (high frequency waves > 1 Hz) mainly produced by human activities (traffic, outside activities etc.…) but also by natural sources such as rivers and wind (about 1 Hz). The first ones are more related to faraway causes rather than microtremors that are related to regional or local sources. For this reason, this latter will be exploited to achieve the objective of the project (Wapenaar 2004).

In most seismic applications steps are taken to remove the effect of the ambient noise, as it acts to obscure other seismic signals which are traditionally used to infer information about the subsurface (usually the P-, S-, and surface waves generated by earthquakes or man-made sources). However, in recent years, it has emerged that ambient noise is far from useless: it has been demonstrated theoretically and in practice that is possible to use ambient noise records at seismometer pairs to reconstruct the seismic response at one receiver as if an active source had been placed at the other (Larose et al. 2015): this process is known as Seismic noise interferometry (SNI) or cross-correlation of ambient seismic noise (IASPEI/IAVCEI Joint Commission on Volcano Seismology - Tutorial 6 - Seismic Noise Interferometry. Retrieved from http://volc_seis_commission.leeds.ac.uk /indexa63d.html).

It has been proved for example that, using ambient noise it is possible to track thermal variations in the subsoil, in buildings or in rock columns, the temporal and spatial evolution of a water table inside landslides, the evolution of the rigidity of the soil constituting a landslide, and especially the drop of rigidity preceding a failure event (Larose et al., 2015).

The principle of seismic noise interferometry is to use ambient seismic noise to calculate noise cross-correlation functions (NCFs) that represent approximations of the Green's function (GF) between seismic stations at different times (Gassenmeier et al., 2014). When changes in the subsurface medium occur during the noise recording period these may be observed in the reconstructed GF and quantified as seismic velocity variations using monitoring methods (Wapenaar et al., 2010). Therefore, in other words, the cross-correlation of ambient noise recordings, made at different locations on a free-surface, theoretically synthesises the seismic energy that would be registered at one of the receiver locations if there had been an impulsive seismic source at the other (IASPEI/IAVCEI Joint Commission on Volcano Seismology - Tutorial 6 - Seismic Noise Interferometry. Retrieved from http://volc_seis_commission.leeds.ac.uk/indexa63d.html). This result is given in terms of Green's function (Figure 24)

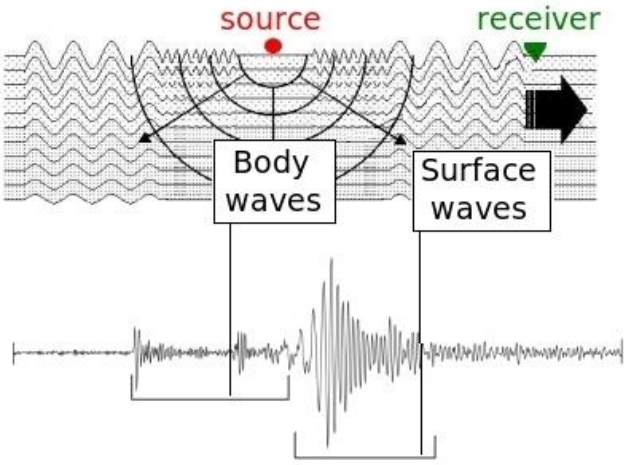

Figure 24. *Representation of a Greens function, which describes the seismic energy (filtered) which would be recorded at a receiver (bottom) in response to an impulsive source (top). Black arrows indicate the direction of wave propagation*

Two examples of this method's applications are given in the two following images. The first one refers to the monitoring of the water table in a deep-seated, slow-moving landslide located in New Zealand (Voisin et al., 2016). The second study case shows the monitoring of environmental influences on seismic velocity at the geological storage site for CO2 in Ketzin (Germany) with ambient seismic noise (Gassenmeier et al., 2014).

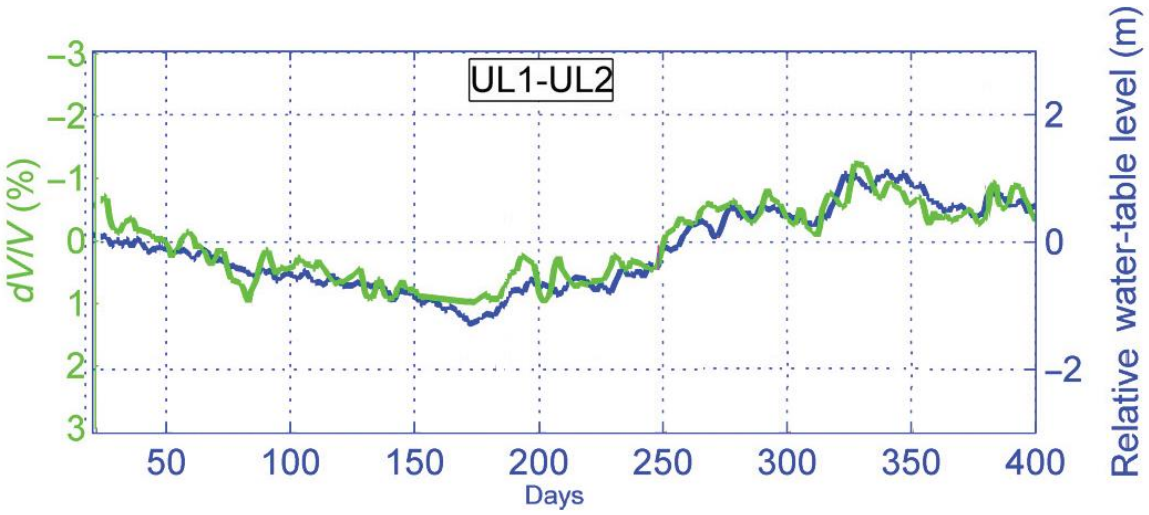

Figure 25. *Utiku landslide case study: Comparison between relative seismic velocity variations (green curve) and absolute pore-pressure measurements (blue curve) for a station pair.*

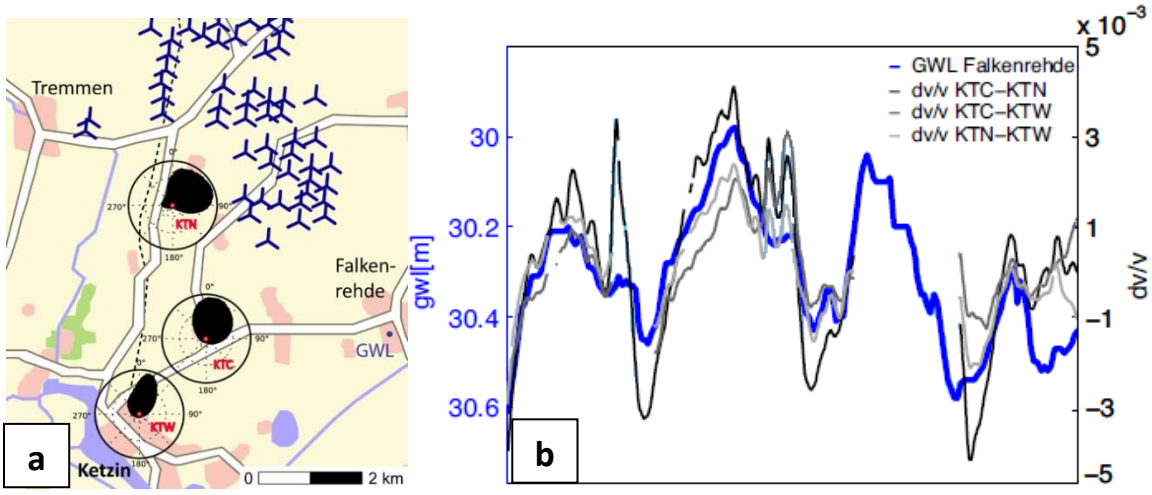

Figure 26. a) *Station map of Ketzin.* ***b)*** *Comparison of velocity change, for different couple of stations (KTC, KTN, KTW), with groundwater level (GWL).*

4.2. Cross Correlation of Ambient Seismic Noise technique

The procedure applied to the recorded ambient seismic noise is outlined in the chart below:

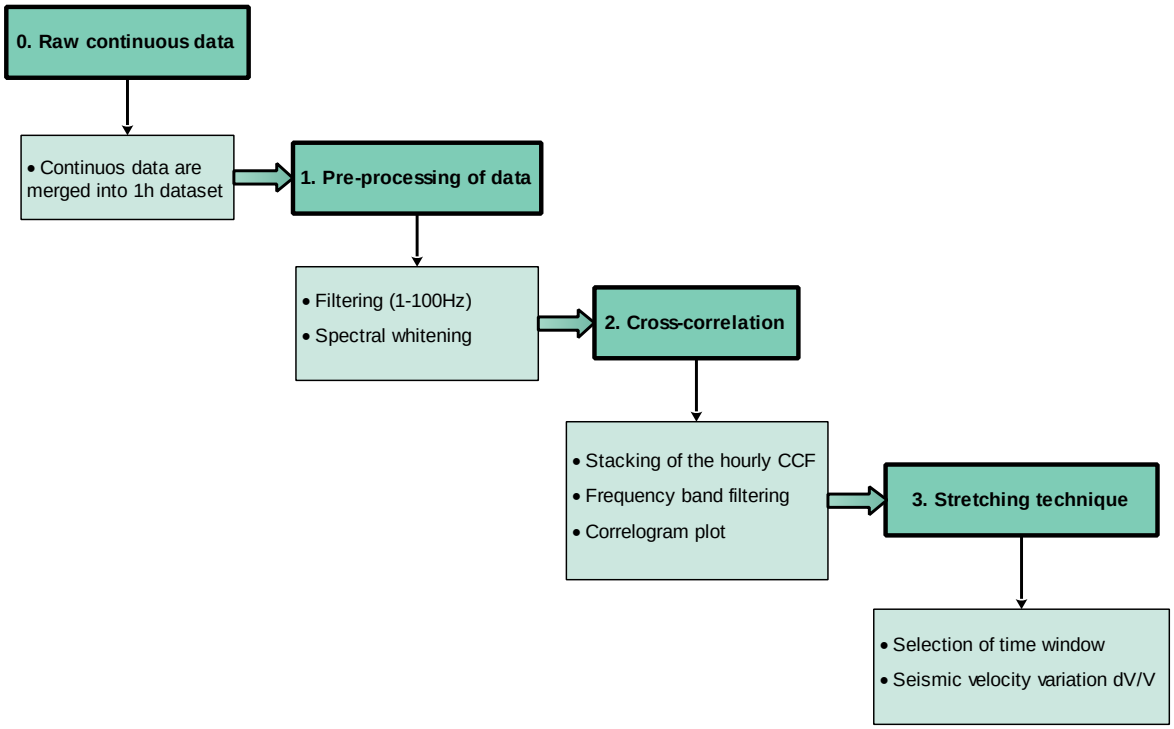

Figure 27. *General workflow to process ambient seismic noise cross-correlation and extract daily relative velocity changes dV/V*

4.2.1. Pre-processing of data

As it can be seen from the scheme, the collected data, that have been merged into 1 hour records and filtered, must be subjected to the spectral whitening. This process, which precedes the cross-correlation, is applied to down-weight the contribution of high-energy arrivals which could obscure the low amplitude ambient noise signal (IASPEI/IAVCEI Joint Commission on Volcano Seismology - Tutorial 6 - Seismic Noise Interferometry. Retrieved from http://volc_seis_commission.leeds.ac.uk/indexa63d.html).

In addition, there is a need to assess the stability of spectral content over time. Indeed, Hadziioannou et al. (2009) demonstrated that noise based monitoring requires a stable source distribution for the full convergence towards the Green's function (Hadziioannou et al., 2011). This phase will be illustrated in "data acquisition and analysis of ambient seismic noise" chapter.

4.2.2. Cross-correlation

Cross-correlation is an operation which measures the similarity of two waveforms by identifying the **time lag** (τ) at which they are most similar. Thus, τ represents the amount which one of the signals is shifted relative to the other. The cross-correlation of two signals **a** and **b**, $C_{a,b}$, is therefore a function of time lag, and is commonly defined as:

$$C_{a,b}(\tau) = \int u(t,a) * u(t-\tau,b)dt$$

where integration is performed over the length of the records, and **u** is the amplitude of a signal as a function of time.

$C_{a,b}$ is maximum when the sum of the product $u(t,a) * u(t-\tau,b)$ is at maximum. This means that a and b are most similar when b is shifted by that amount relative to a. An auto-correlation (cross-correlation of a signal with itself) therefore has its maximum at a time lag of zero.

A useful way to understand the role of cross-correlation in SNI is that it highlights the travel-times of seismic waves. A wave-field which has travelled between two stations (A-B) will cause a similar signal to be recorded at each, shifted in time: the cross-correlation function (CCF) of the records will therefore contain a peak at a time lag which corresponds to the travel time of the wavefield between the two stations (Figure 28) (IASPEI/IAVCEI Joint Commission on Volcano Seismology - Tutorial 6 - Seismic Noise Interferometry. Retrieved from http://volc_seis_commission.leeds.ac.uk/indexa63d.html).

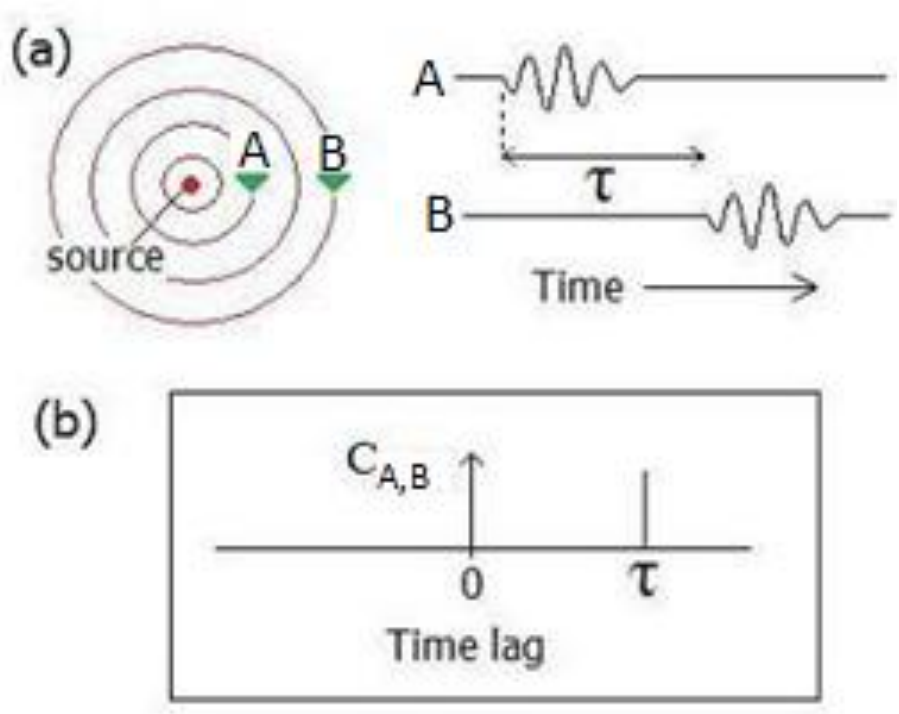

Figure 28. *(a) A source of seismic energy (left) is recorded at receivers A and B, causing identical signals separated by a time τ (right), corresponding to the travel time of the wavefield between the receivers. (b) the cross-correlation function of the two records, on which the traveltime is highlighted as a peak.*

Cross-correlation is performed for positive and negative time lags, so CCFs have both positive ("causal") and negative ("acausal") parts. Ambient seismic noise arrives from all directions, and the noise records, which are cross-correlated during SNI, contain energy which has travelled in both directions along an interstation path. Green's function, which emerge on noise cross-correlation functions (NCFs), will therefore contain energy in both the causal and acausal parts, symmetric about zero time lag: the causal part represent energy travelling from station A to station B, and the acausal part energy arriving at station A from station B (Figure 29) (IASPEI/IAVCEI Joint Commission on Volcano Seismology - Tutorial 6 - Seismic Noise Interferometry. Retrieved from http://volc_seis_commission.leeds.ac.uk/indexa63d.html).

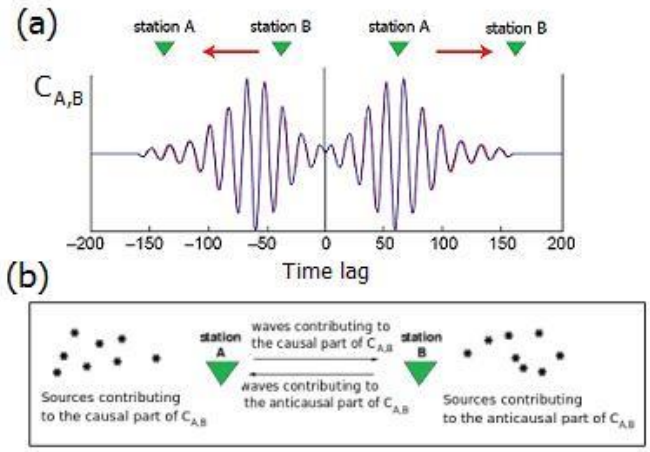

Figure 29. *Causal and anticausal parts of an NCF. (a) Idealised NCF for the cross-correlation order station A to station B. The arrows indicate the energy path which is represented by the positive and negative parts of the cross-correlation function. (b) Representation of the noise sources which (theoretically) contribute to the causal and anticausal part of the station A - station B NCF.*

Because GFs are usually assumed to be the same in both directions along a path, the two sides of an NCF can be treated as representing exactly the same information, but reversed in time. In reality NCFs will be perfectly symmetrical only if noise arrives from both side of the interstation path with a strength as similar as possible. Therefore, the symmetry is possible depending on the noise sources distribution. This condition is usually difficult to obtain because the source of ambient seismic noise is usually anisotropy (IASPEI/IAVCEI Joint Commission on Volcano Seismology - Tutorial 6 - Seismic Noise Interferometry. Retrieved from http://volc_seis_commission.leeds.ac.uk/indexa63d.html). However the necessary assumption is that the noise sources are stable over time (Hadziioannou et al. 2011).

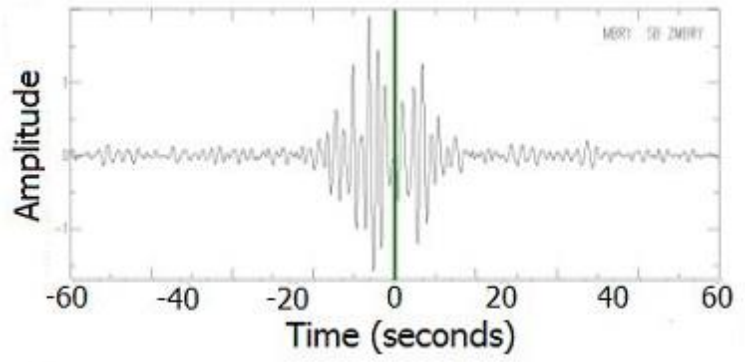

Figure 30. *Daily noise cross-correlation example. Note the asymmetry due to source anisotropy. In the upper part it is possible to see more energy propagate to one direction respect to the other (left side).*

After this process, the daily cross-correlation are stacked over the whole time monitoring period and subjected to a frequency band filtering. This must be done because, for example, the property of the analysed surface waves is that low frequency waves investigate deeper than higher frequency waves that propagate closer to surface. Therefore, for a specific depth, there will be a specific wave field corresponding to a specific frequency band leading to water table variation characterisation. The resulting stacked and filtered daily cross-correlations are then put in sequence into a correlogram where the x axis represents the time lag and in y axis the period with all the daily correlations expressed in amplitude of the phases (Graph 4).

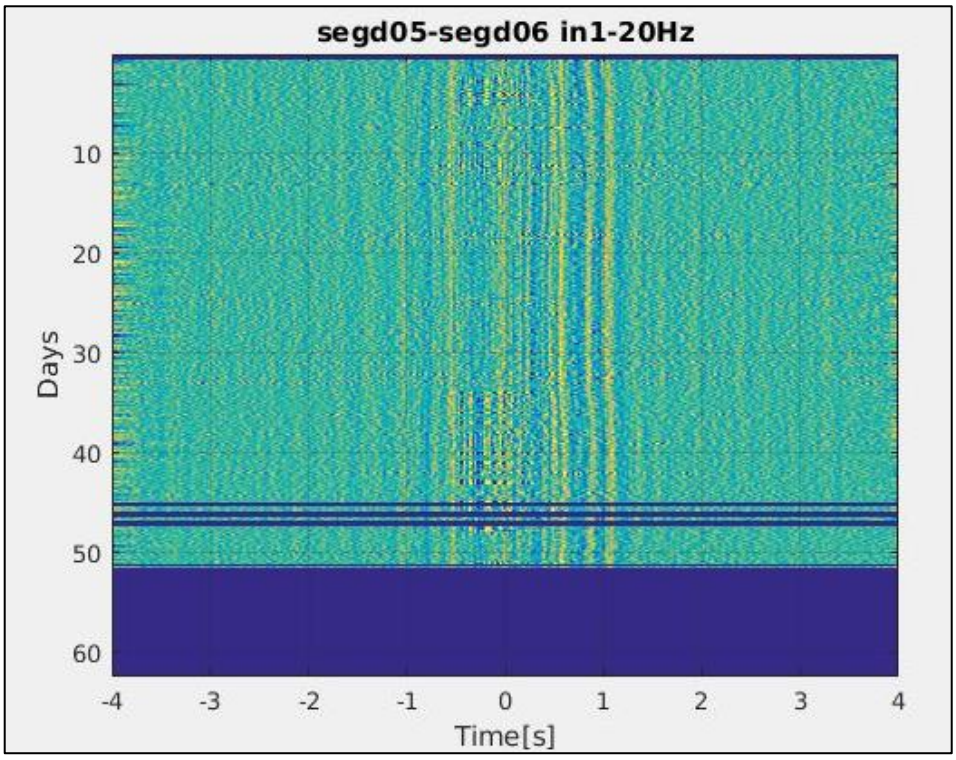

Graph 4. *Broadband correlogram resulting from the cross correlation of the vertical components of the stations' couple 5-6. The light blue horizontal bands are missing data. It is possible to see the stability of arrivals confirming the temporal stability of the noise sources. However, this feature will be also verify with the spectrogram in paragraph 4.3.*

4.2.3. Stretching technique

Once the recorded data have been cross-correlated and plotted into a correlogram, the seismic velocity variation can be computed. This procedure consists on using stretching technique that is particularly appropriate to detect localised velocity variations rather than doublet technique (Sens-Schönfelder and Wegler, 2006). Even if this process follows the same procedure deployed for Utiku landslide in New Zealand (Voisin et al., 2016), it has been necessary to realize a new code for the particular case of the thesis' project (appendix 2). This procedure requires the definition of a *reference* correlation that is computed by averaging all of the correlations over the duration of the experiment. In a

second step a time window is selected in the correlogram, within the lapse time range of interest, to compute the velocity variations. For each hour, the time vector t of the correlation is multiplied by a stretching factor e, i.e., $t \leftarrow t \times (1+e)$ to align the arrival time of the seismic phases, within the selected time window, to the arrival time of reference. Many different values of the stretching factor e are tested. The one retained is the one that maximizes the cross-correlation coefficient (CC) between the *reference* and the hourly cross-correlation. The stretching factor e could be either positive (i.e., the seismic phases arrive later than their reference time) or negative (i.e., the seismic phases arrive before their reference time) (Voisin et al. 2016).
The CC between the stretched correlation and the reference one is computed as:

$$CC(\varepsilon) = \frac{\int_{t_1}^{t_2} h\left[t(1-\varepsilon)\right] h_0[t]dt}{\sqrt{\int_{t_1}^{t_2} h^2\left[t(1-\varepsilon)\right] dt . \int_{t_1}^{t_2} h_0^2[t]dt}}$$

where:
-t_1 and t_2 are the limits of the selected time window;
-h(t) is the stretched correlation;
-h_0(t) is the reference;

Finally, the seismic velocity change curve is defined as the opposite of the vector of the hourly maximum stretching factor.

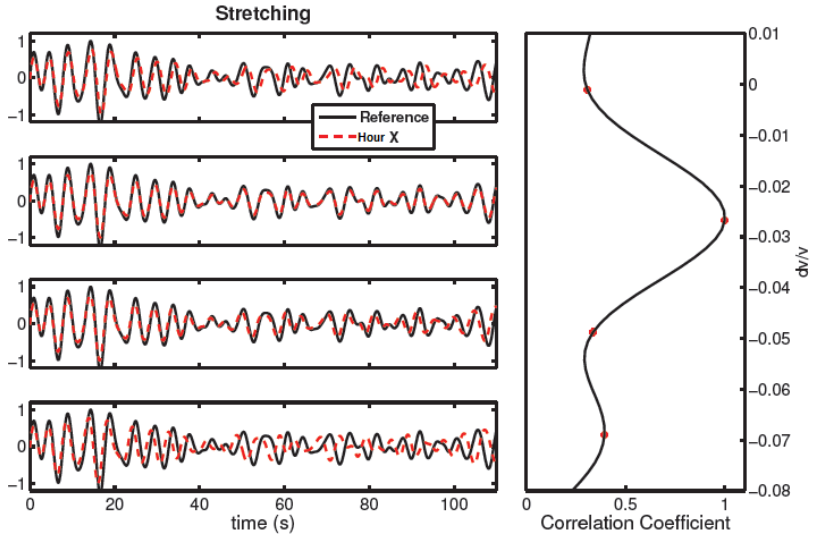

***Figure 31**. Stretching method: physical understanding. Left: The signal is stretched for different e values. Right: Coefficient correlation between the signal (red) and the reference (black) are calculated for every test daily signals.*

Once the seismic velocity variations are computed, it is necessary to compare it with groundwater table level in order to establish correlations hence assessing the goodness of the method. The procedure has been applied for those stations that are at the opposite sides of the basin: station pairs 5-6, 4-7, 3-8, 2-9, 1-10 (Figure 32). This choice allows to compare the obtained result of each single case with the same piezometer (P96) located at the centre of infiltration basin. The others piezometer data have not been considered because they show the same fluctuations of the selected one (P96). The only difference among them, as can be seen in graph 2b, is a scale factor that depends on the distance between the piezometer and the infiltration basin (piezometers far from the basin, show lower water level respect to those closer). However, this assumption does not affect our objective since velocity variations and groundwater level have different unit of measure and therefore a standardization of both data it is necessary before to compare the two curves.

4.3. Data acquisition and analysis of ambient seismic noise

For the monitoring of groundwater level in Crépieux-Charmy, ten seismic stations were placed on both sides of the basin 5-2 on 30th November 2016 (figure 32). Each of these were connected to a 5Hz three-component geophone (SG-5), recording ambient seismic noise continuously at 250 Hz sampling rate. In order to extend the working autonomy of the internal stations battery, it has been decided to add an external one coupled to a solar panel.

Figure 32. *Map of the studied area and locations of seismological stations and ambient seismic sources.*

As already said, the cross-correlation technique works best when the noise distribution is uniform in space and time (Larose et al., 2004; Roux et al., 2005; Shapiro and Campillo, 2004; Snieder, 2004). Therefore it is necessary to do an analysis of the seismic sources.
From direct observations during the field experiments, three main sources of ambient noise were identified: the river's channels, the traffic along the highway and the railway. The stations have been installed aligned to the basin in order to be, as much as possible,

perpendicular to these passive sources. This choice leads to a better reconstruction of seismic velocity variations.

When the noise sources are uniformly distributed, it can be mathematically proven that the cross-correlation of noise records at two nearby receivers is symmetrical about the zero lag time and equivalent to the Green's function (Snieder, 2004). In fact, the existence of dominant ambient noise sources presents a major element of uncertainty. For instance, strong tides can directly affect the accuracy of the results (van Dalen et al., 2015).

The vertical-component correlation functions computed for all station pairs exhibit distance-time *moveouts* that are consistent with Rayleigh waves propagating from one station to another (Graph 5). For the selected frequency range (1-5Hz), the delay (lag) times of the correlation peaks accurately reflect the Rayleigh wave phase velocity between the respective station pairs (Gu et al., 2009).

The obtained noise cross-correlation functions (Graph 5) are almost perfectly symmetrical, meaning that the noise arrives from both side of the interstation path with a very similar strength.

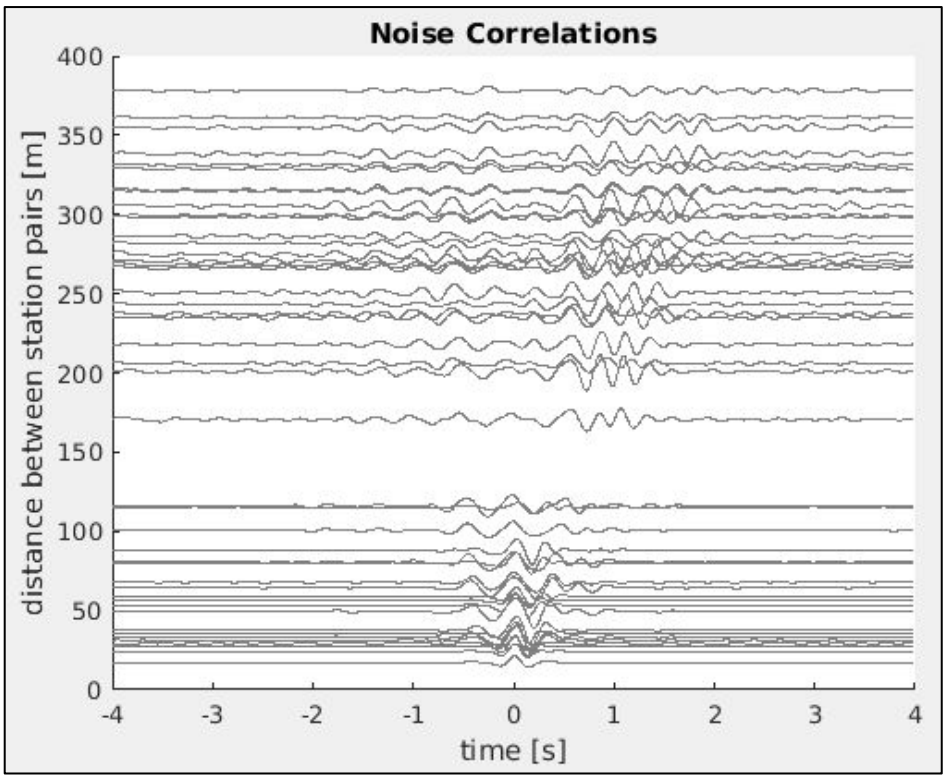

Graph 5. *Vertical-component cross-correlation functions of seismic noise, computed from a two months station recordings. A band-pass filter (1-5Hz) has been applied to the original cross-correlation functions.*

A further requirement to better converge towards the Green's function, is the stability of noise sources distribution over time (Hadziioannou et al. 2011). To ensure this feature it is necessary to investigate the spectral content of noise field and its stationarity (Gassenmeier et al. 2014). This analysis has been done calculating the spectrogram of the vertical component of each station. The obtained results (Graph 6 refers to station 5) show that the noise sources' pattern remains stable over time (Gassenmeier et al. 2014). For monitoring purposes this spectral stability is very important because its lack can introduce artefacts in measurements of velocity variations (Zhan et al., 2013).
Another way to verify this property can be done looking at the correlogram. In fact, as shown in graph 4, the continuity over time of the visible arrivals for the station pair 5-6 ensure that this required condition is satisfied.

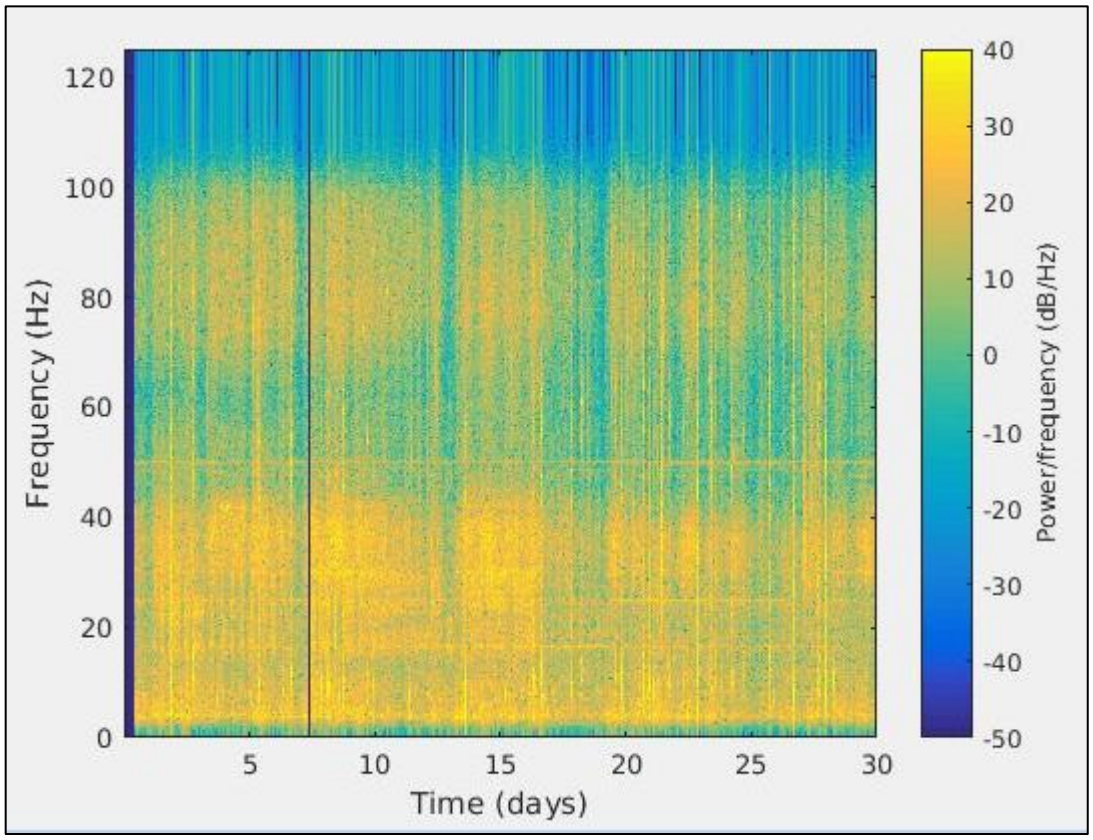

Graph 6. *Spectrogram of station n° 5.*

4.4. Results

The processing of the retrieved data leads to the following results. The first figure is obtained considering the station pair 5-6 and the broadband frequency, i.e., 1-20Hz. The blue line represents the groundwater level recorded at the reference piezometer P96. The comparison with the seismic velocity variations (magenta line) is striking (Graph 7). The two physical and independent measurements are strongly correlated over the almost two months of the experiment.

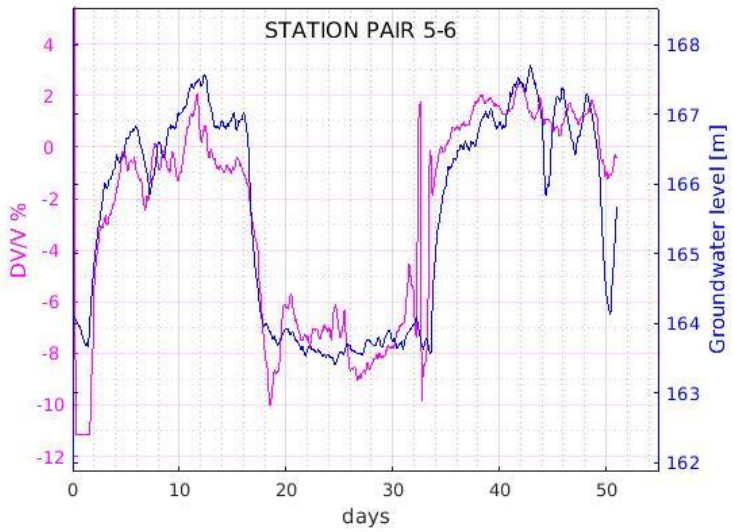

Graph 7. *Station pair 5-6: comparison between seismic velocity changes and groundwater level computed for broadband frequency range (1-20Hz).*

In order to assess at which frequency range the velocity changes are more sensitive to the groundwater level, the cross-correlation technique has been computed for different frequency bandwidths. This procedure, that aims to investigate different depths, has been done for all the studied station pairs as presented in graph 8. It can be observed that the green curve, representing the dV/V, does not cover all 51 days of monitoring (excepted for station pair 5-6). This lack of data is due to the cold winter which caused a decay of station's battery (appendix 3 shows the percentage of functioning days for each seismic station). However this does not affect the computed velocity variation.
The frequency ranges for which we are able to better detect water table changes are:

Station pair	Distance [m]	Frequency bandwidth [Hz]
5-6	170.6	10-12
4-7	234.9	10-11
3-8	281.8	9-10
2-9	338.2	8-9
1-10	378.2	6-7

Table 3. *Frequency bandwidth for which it is possible to detect groundwater level changes.*

From these values it seems that there is a clear relationship between the frequency bandwidth and the distance between the stations. In fact, for a bigger distance it corresponds a lower frequency' value meaning that water variations are detected at a deeper depth. Due to the fact that the distance between the stations is also directly proportional to the distance from the infiltration basin, it is interesting to evaluate if, in the piezometers further from the infiltration basin, the groundwater level is deeper than those closer to it. Looking at graph 2b this assumption can be confirmed, in fact it is clearly visible that the water level varies according to the distance between the piezometer and the infiltration basin. For example, the piezometer S03, which is the furthest one from the infiltration basin shows the deepest groundwater level. The same result, but in term of frequency bandwidth, is obtained for the cross-correlation computed for sensors 1 (next to piezometer S03) and 10 which are the furthest from the infiltration basin.
However, even if these results seem consistent, further tests must be done to verify with reasonable certainty these conclusions.

Another thing that can be observed (Graph 8), function of the distance between the station pairs, is the fact that seismic velocity changes seems to be more correlated with groundwater level when the distance between the sensors is smaller.
In order to verify this hypothesis it has been calculated, for each plot, the correlation coefficient (CC) between the two curves:

Station pair	Distance [m]	CC
5-6	170.6	0.813
4-7	234.9	0.867
3-8	281.8	0.867
2-9	338.2	0.520
1-10	378.2	0.719

Table 4. *Correlation coefficient between dV/V and groundwater level computed for each couple of station.*

As it can be seen from the table, the obtained dV/V do not depend on the distance between the pair of stations. Therefore, our assumption is that the quality of dV/V depends on the stations pair position: the more the stations are perpendicular to the source of noise, the better will be the obtained result. However this is a hypothesis and additional researches are necessary to better understand which location and distance between stations leads to the best result.

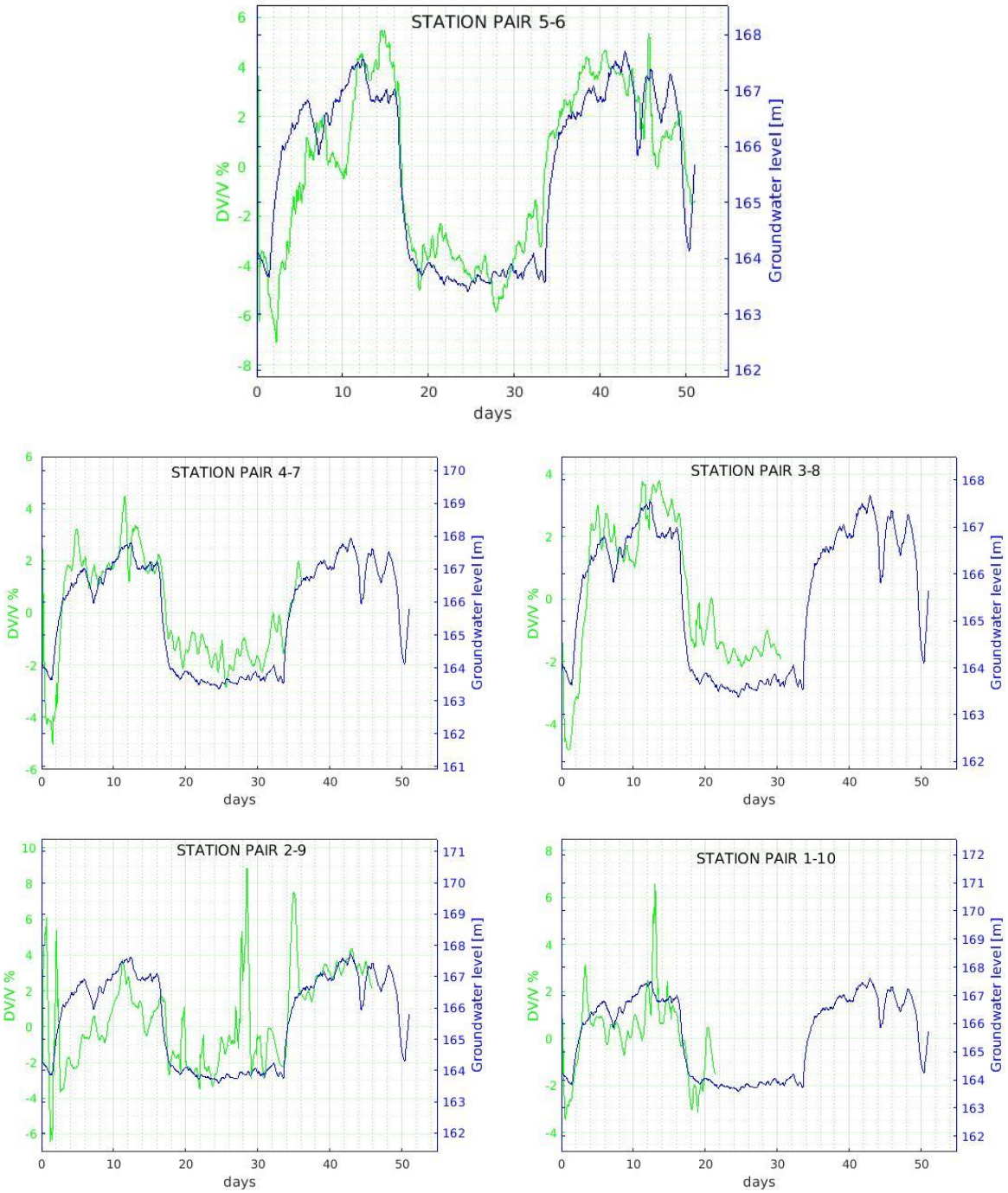

Graph 8. *Comparison between velocity variations (green curves) and groundwater level (blue curves) for station pairs 5-6, 4-7, 3-8, 2-9 and 1-10, respectively. Note the good agreement for almost all station pairs. Because of missing data, only DV/V for station pair 5-6 covers all 51 days of monitoring.*

From the above graphs it can be also observed that the seismic velocity changes for each pair of stations are in phase, even if, for the furthest ones, there are some noises. This is a confirmation that changes depend on the same phenomena that affect the entire study area: the groundwater variations. In fact, each seismic velocity change curve follows the piezometers behaviour, confirming a strong relation between the two physical and independent measurements (Voisin et al., 2016).

In order to verify if the seismic stations could be a reliable substitute of the piezometers, which means savings in terms of time and costs, the cross-correlation technique has been also applied to station pair 6-7. The latter have been chosen according to the fact that these two stations are the nearest ones (35 m) and with the biggest amount of recorded data.

The obtained results, both in the broadband and into 8-12 Hz frequency band (Graph 9), provide a satisficing correlation between the velocity variations and the aquifer level changes.

Even if satisfying result have been achieved this research is still in a preliminary phase and we are far from concluding that seismic stations can substitute the piezometers. Furthermore it must be keep in mind that it is still not possible to obtain these results using only one single station, and that, in order to use this technique for the monitoring of the groundwater variations, it will be necessary to periodically check and calibrate the obtained measurements to ensure the reliability of the system.

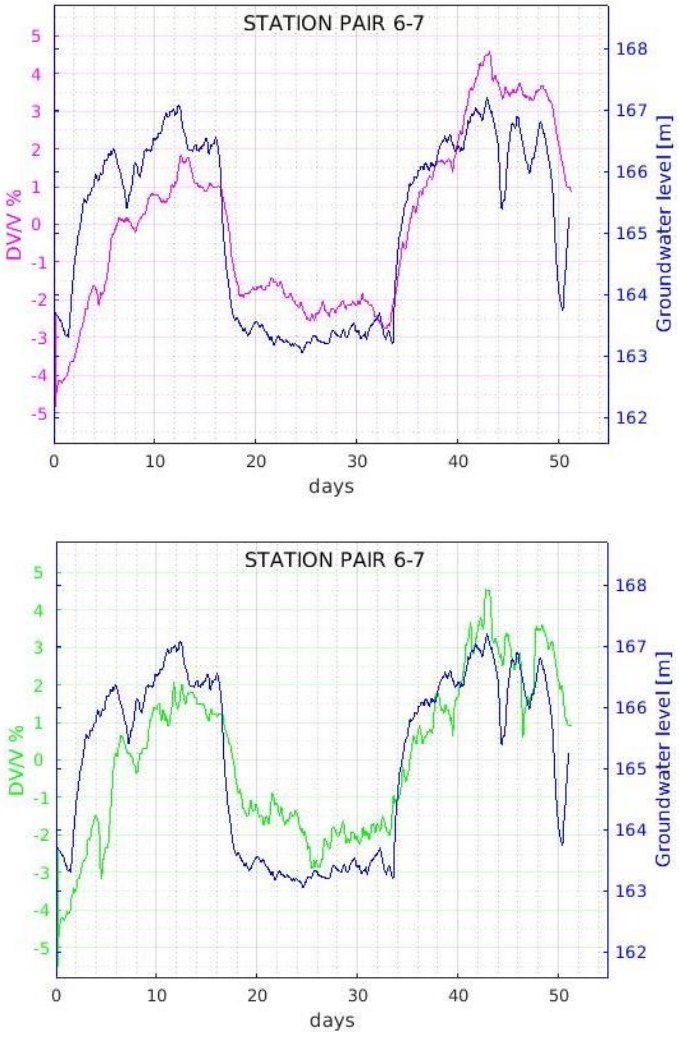

Graph 9. *Comparison between seismic velocity changes and groundwater level computed for broadband frequency range (magenta curve) and for frequency range 8-12Hz (green curve).*

In order to better address the problem of localization of the change in the medium, the seismic velocity variations derived for limited frequency bandwidths are compared with those obtained from the broadest frequency bandwidth (1-20 Hz), which is used as a reference. The comparison is achieved by computing the autocorrelation of the 1-20 Hz seismic velocity curve and the cross-correlation of the 1-20 Hz seismic velocity curve with the 6–8, 8–10,12-14 and 16-18 Hz seismic variation curves, respectively. Graph 9 shows the results for the station pair 5-6. First, it is important to note that all limited spectral bandwidths exhibit velocity variations. However, the velocity variations computed within the 6–8 and 8-10 Hz frequency range match the broadband reference computed over the 1-20 Hz band. The other frequency bands provide seismic velocity variations that do not match the reference seismic velocity variations and/or are not in phase with the monthly pattern. We conclude that (1) the 6-8 and 8-10 Hz frequency bands bear the pattern and (2) the physical process causing the seismic velocity variations does not affect the entire volume of the study area (in which case, all limited spectral bandwidth velocity variations would look similar to each other), but rather originates from localized changes occurring at some depth, due to the groundwater level (Voisin et al. 2016).

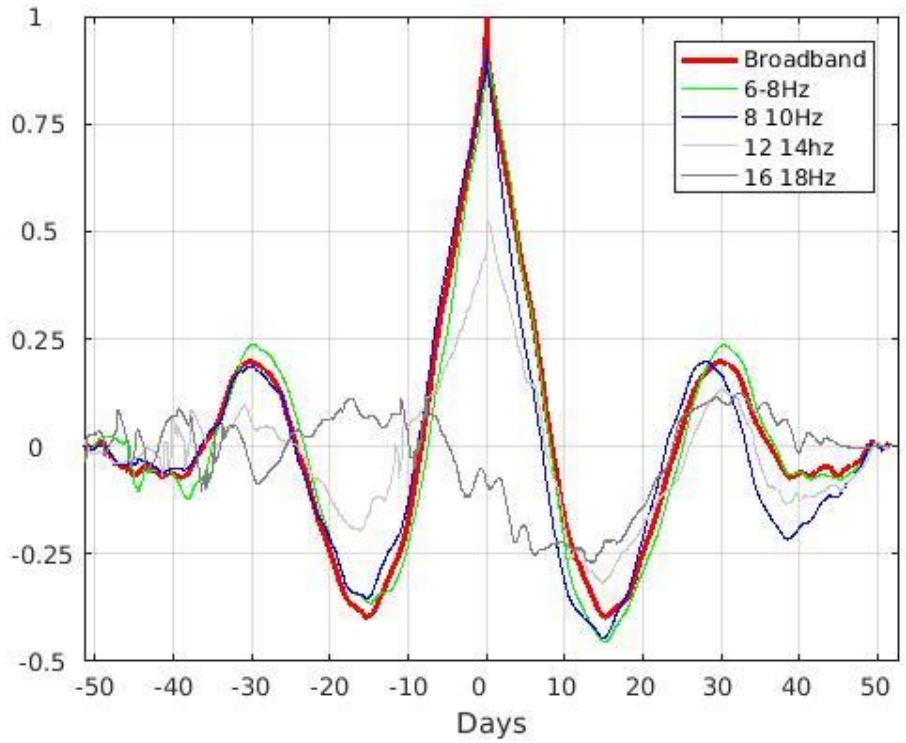

Graph 10. *Comparison of the autocorrelation of broadband velocity variations (magenta curve of Graph 7 autocorrelated to give the reference in red) with the crosscorrelation of broadband velocity variation and band limited velocity variation. The 16-18 Hz bandwidth has little in common with the broadband velocity variation and bears no clear monthly signal. On the other hand, the 12-14 Hz bandwidth is apparently in phase with the reference, but the crosscorrelation does not fit the reference curve. The best match is obtained for the 6–8 and 8-10 Hz bandwidth that bears most of the environmental signal, and it is in-phase with the broadband velocity variations (i.e., with the groundwater level measurements).*

5. Conclusions

The aim of this thesis was to extend the applicability of the cross-correlation of ambient seismic noise technique for the monitoring of those areas where the subsurface properties, in this case the water content, do not follow the natural processes because they are strongly influenced by the human activities.

This methodology, which has been applied to the Crépieux-Charmy water capturing field, showed clear variations in seismic velocities. It has been firstly verified that these variations were not caused by changes in the characteristics of the noise field, checking whether the latter was both stable over space and time. Once this has been verified, we analysed the data collected in the piezometers in order to understand the reasons of the velocity changes. The latter's curve demonstrated a striking match with the groundwater level in each studied couple of station, even if, for those further, there are some noises.

After this interpretative phase it was then necessary to evaluate which frequency bandwidth was more sensitive to the groundwater fluctuations and thus, to obtain the best match between the velocity variations' curve and the aquifer's one. The obtained frequency ranges have shown a direct dependence with the distance between the studied station pairs. In particular, bigger distances corresponded to the lower frequencies and therefore to greater depths. We thus checked whether this trend was also visible in the data collected by piezometers. Although this link has been positively identified, deeper studies are necessary to ensure the full truthfulness of this information.

In the perspective of demonstrating that the seismic stations could become an efficient alternative to the piezometers for the continue monitor of groundwater level, the cross-correlation technique has been then applied to two close seismic stations. Even if satisfying results have been achieved this research is still in a preliminary phase.

Finally, a further check has been done to demonstrate that the better correlation between velocity changes and groundwater level is borne by a limited frequency band (6-10 Hz typically). Also this verification led to satisfactory results, showing that outside of this frequency range we lose information about the aquifer.

Therefore, it can be concluded that this technique is sensitive to the unnatural oscillations of the water table and it has a considerable potential for the assessment of underground water resources (Voisin et al. 2016). Unfortunately, it is not yet possible to say that this technique can be used as a non-destructive hydrologic monitoring tool, because the correlation between velocity variations and groundwater table depth is not yet been achieved. To overcome this problem it will be interesting to develop the sensitivity kernel which relates the mean travel time changes to the localized relative velocity change within the subsurface (Kanu and Snieder, 2014). This is achievable if it assumed that the seismic phases used to compute the relative velocity changes are Rayleigh waves. Given

the nature of the noise sources in this study (trains, cars and river), this assumption seems reasonable and therefore this method could bring to a satisfactory result (Voisin et al., 2016).
A different method, that could be applied for the same purpose, consists in looking at the depth of maximum surface-wave energy in the analysed frequency bands (Graff, 1975).
If one of these solutions will yield to satisfactory results, the future idea is to develop a complete three-dimensional groundwater monitoring system for the water capturing field. This will allow to localize the bulge under each basin and therefore to ensure compliance with the two meters of unsaturated zone. Furthermore it will be also possible to guarantee the effective functioning of the hydraulic barrier against potential pollutant.

In conclusion, it may be said that this technique seems to provide an excellent starting point for the development of a continuous water monitoring system. An adequate management of the resource could contribute to sustainable exploitation and foresee drought and flood incidents. The assessment of the volume of groundwater available as well as the extent of exhaustion and reconstruction at the local/regional level is a difficult but mandatory task for the sustainable development of our human activities. In this task, we have seen that geophysics, and more precisely seismology, could be a precious instrument also in terms of saving money and time.

In addition to hydrologic monitoring applications, this technique offers potential in those fields in which water table variations can control dynamics of different events. For instance it could be used for landslides or rock-fall monitoring, where water plays the role of triggering factor. Indeed, thanks to the fact that the physics of wave propagation is scale independent and because of the high sensitivity of the noise monitoring technique, one can imagine other seismic noise experiments applied to monitoring these kind of events (Voisin et al. 2016). Predicting these sudden events, primarily controlled by groundwater conditions, has been an active research topic for the last two decades (Lee and Ho, 2009). At a larger scale, with lower frequencies, this technique can also be used to monitor any fluid substitution changes, even if the seismic wavefield is composed of volume waves.

References:

Astiz, Luciana, Paul Earle, and Peter Shearer
1996 Global Stacking of Broadband Seismograms. Seismological Research Letters 67(4): 8–18.

Bonneton, Jacquemard, and Taxil
2016 Prospection Gèophysique.

Brenguier, Florent, Nikolai M. Shapiro, Michel Campillo, et al.
2008 Towards Forecasting Volcanic Eruptions Using Seismic Noise. Nature Geoscience 1(2): 126–130.

van Dalen, Karel N., T. Dylan Mikesell, Elmer N. Ruigrok, and Kees Wapenaar
2015 Retrieving Surface Waves from Ambient Seismic Noise Using Seismic Interferometry by Multidimensional Deconvolution. Journal of Geophysical Research: Solid Earth 120(2): 944–961.

Electrical Resistivity Tomography (ERT)
N.d. TerraDat UK Ltd. http://terradat.co.uk/survey-methods/resistivity-tomography/, accessed June 28, 2017.

Gassenmeier, M., C. Sens-Schonfelder, M. Delatre, and M. Korn
2014 Monitoring of Environmental Influences on Seismic Velocity at the Geological Storage Site for CO2 in Ketzin (Germany) with Ambient Seismic Noise. Geophysical Journal International 200(1): 524–533.

Graff, K.L. (1975) Wave Motion in Elastic Solids. Ohio State University Press, Belfast, Ireland. - References - Scientific Research Publish
N.d.
http://www.scirp.org/(S(lz5mqp453edsnp55rrgjct55))/reference/ReferencesPapers.aspx?ReferenceID=1852782, accessed June 30, 2017.

Gu, Yu Jeffrey, Ahmet Okeler, Sean Contenti, et al.
2009 Broadband Seismic Array Deployment and Data Analysis in Alberta. CSEG Recorder, September: 37–44.

Hadziioannou, Céline, Eric Larose, Adam Baig, Philippe Roux, and Michel Campillo
2011 Improving Temporal Resolution in Ambient Noise Monitoring of Seismic Wave Speed. Journal of Geophysical Research: Solid Earth 116(B7). http://onlinelibrary.wiley.com/doi/10.1029/2011JB008200/full, accessed June 28, 2017.

Hilbich, C., C. Hauck, M. Hoelzle, et al.
2008 Monitoring Mountain Permafrost Evolution Using Electrical Resistivity Tomography: A 7-Year Study of Seasonal, Annual, and Long-Term Variations at Schilthorn, Swiss Alps. Journal of Geophysical Research 113(F1). http://doi.wiley.com/10.1029/2007JF000799, accessed June 28, 2017.

IASPEI/IAVCEI Joint Commission on Volcano Seismology - Tutorial 6 - Seismic Noise Interferometry
N.d.
http://volc_seis_commission.leeds.ac.uk/index3d3a.html?option=com_content&task=view&id=75&Itemid=44., accessed July 5, 2017.

Kanu, Chinaemerem, and Roel Snieder
2014 Numerical Computation of the Sensitivity Kernel for Time-Lapse Monitoring with Multiply Scattered Waves. Center for Wave Phenomena Rep 816: 291–306.

Larose, Eric, Simon Carrière, Christophe Voisin, et al.
2015 Environmental Seismology: What Can We Learn on Earth Surface Processes with Ambient Noise? Journal of Applied Geophysics 116: 62–74.

Larose, Eric, Arnaud Derode, Michel Campillo, and Mathias Fink
2004 Imaging from One-Bit Correlations of Wideband Diffuse Wave Fields. Journal of Applied Physics 95(12): 8393–8399.

Lee, Kwan Tun, and Jui-Yi Ho
2009 Prediction of Landslide Occurrence Based on Slope-Instability Analysis and Hydrological Model Simulation. Journal of Hydrology 375(3–4): 489–497.

Loizeau, Sébastien
2013 Amélioration de La Compréhension Des Fonctionnements Hydrodynamiques Du Champ Captant de Crépieux-Charmy. Université de Grenoble. https://hal.archives-ouvertes.fr/tel-00849117/, accessed June 26, 2017.

Mainsant, Guénolé, Eric Larose, Cornelia Brönnimann, et al.
2012 Ambient Seismic Noise Monitoring of a Clay Landslide: Toward Failure Prediction: SEISMIC NOISE MONITORING OF A LANDSLIDE. Journal of Geophysical Research: Earth Surface 117(F1): n/a-n/a.

Mordret, Aur?lien, Nikola? M. Shapiro, and Satish Singh
2014 Seismic Noise-Based Time-Lapse Monitoring of the Valhall Overburden. Geophysical Research Letters 41(14): 4945–4952.

Ratdomopurbo, Antonius, and Georges Poupinet
1995 Monitoring a Temporal Change of Seismic Velocity in a Volcano: Application to the 1992 Eruption of Mt. Merapi (Indonesia). Geophysical Research Letters (ISSN 0094-8276), vol. 22, no. 7, p. 775-778 (GeoRL Homepage).

Roux, Philippe, Karim G. Sabra, W. A. Kuperman, and Andre Roux
2005 Ambient Noise Cross Correlation in Free Space: Theoretical Approach. The Journal of the Acoustical Society of America 117(1): 79–84.

Seismic Acquisition Introduction | Reflection Seismology | Sampling (Signal Processing)
N.d. Scribd. https://www.scribd.com/document/154707054/Seismic-Acquisition-Introduction, accessed June 28, 2017.

Seismic Tomography
2017 Wikipedia. https://en.wikipedia.org/w/index.php?title=Seismic_tomography&oldid=784907512.

Sens-Schönfelder, C., and U. Wegler
2006 Passive Image Interferometry and Seasonal Variations of Seismic Velocities at Merapi Volcano, Indonesia. Geophysical Research Letters 33(21). http://doi.wiley.com/10.1029/2006GL027797, accessed May 25, 2017.

Shapiro, N. M., and M. Campillo
2004 Emergence of Broadband Rayleigh Waves from Correlations of the Ambient Seismic Noise: CORRELATIONS OF THE SEISMIC NOISE. Geophysical Research Letters 31(7): n/a-n/a.

Snieder, Roel
2004 Extracting the Green?s Function from the Correlation of Coda Waves: A Derivation Based on Stationary Phase. Physical Review E 69(4). https://link.aps.org/doi/10.1103/PhysRevE.69.046610, accessed June 28, 2017.

Voisin, Christophe, Stéphane Garambois, Chris Massey, and Romain Brossier
2016 Seismic Noise Monitoring of the Water Table in a Deep-Seated, Slow-Moving Landslide. Interpretation 4(3): SJ67-SJ76.

Wapenaar, Kees
2004 Retrieving the Elastodynamic Green's Function of an Arbitrary Inhomogeneous Medium by Cross Correlation. Physical Review Letters 93(25). https://link.aps.org/doi/10.1103/PhysRevLett.93.254301, accessed June 28, 2017.

Wapenaar, Kees, Deyan Draganov, Roel Snieder, Xander Campman, and Arie Verdel
2010 Tutorial on Seismic Interferometry: Part 1 — Basic Principles and Applications. GEOPHYSICS 75(5): 75A195-75A209.

Wylie, Robin
N.d. Tutorial 6 - Seismic Noise Interferometry. IASPEI/IAVCEI Joint Commission on Volcano Seismology. http://volc_seis_commission.leeds.ac.uk/index3d3a.html?option=com_content&task=view&id=75&Itemid=44.

Zhan, Z., V. C. Tsai, and R. W. Clayton
2013 Spurious Velocity Changes Caused by Temporal Variations in Ambient Noise Frequency Content. Geophysical Journal International 194(3): 1574–1581.

Appendix 1

Morphological evolution of Miribel-Jonage Island (Poinsard, 1992)

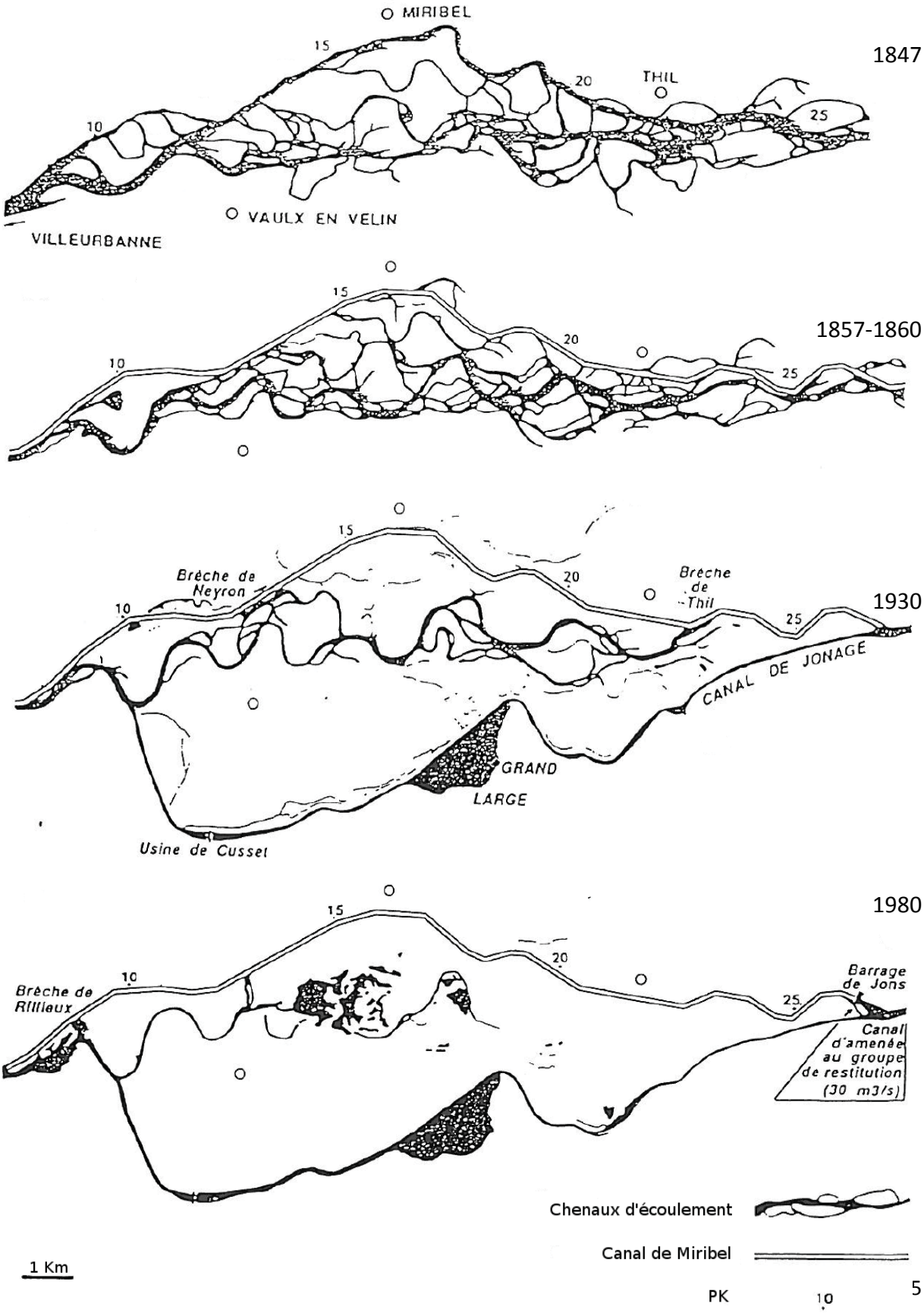

Appendix 2

The following Matlab script has been written in order to apply the stretching technique to the already computed cross-correlations. Its outcome is therefore the velocity variation of wave propagation.

```
Load of the RESU matrix which contains the already computed cross-
correlations. load('segd05_segd06_1_100_whiten.mat')

PLOT OF THE CORRELOGRAM IN POINTS
figure
DFc1=1;
DFc2=20;
ordre=4;
[b,a]=butter(ordre,[DFc1 DFc2]/250*2);
imagesc(filtfilt(b,a,test_fin)')
grid on
title(['segd05-segd06 in' num2str(DFc1) '-' num2str(DFc2) 'Hz' ])

PLOT OF THE CORRELOGRAM IN SECONDS FOR THE SELECTION OF THE TIME WINDOW
fe=250;
ordre=4;
[v,u]=butter(ordre,[DFc1 DFc2]*2/fe);
RESU=filtfilt(v,u,test_fin);
figure
imagesc([-
size(test_fin,1)/2:size(test_fin,1)/2]/fe,[1:size(RESU,2)]/24,RESU');draw
now
grid on
%colormap(jet)
caxis([-0.03,0.01])
title(['segd05-segd06 in' num2str(DFc1) '-' num2str(DFc2) 'Hz' ])


INPUT DATA
Fc1=1;
Fc2=100;
lasthour=1234; %SERVE PER DIRE FINO A CHE ORA HAI I DATI
%Distance=270.48;
%Vmin=350;
%Vmax=450;
%t1=round((Distance/Vmax)*100)/100;
%t2=round((Distance/Vmin)*100)/100;
t1=0.4;
t2=1.2;
sta1='segd05';
sta2='segd06';

currentdir=[num2str(Fc1) '_' num2str(Fc2) 'Hz'];
lisse=31;
seuil=.0; %(0-1)
fe=250;
```

```
ordre=4;
RESU=test_fin(:,1:lasthour);
RESU(find(isnan(RESU)))=0;

PREPROCESSING BEFORE EVALUATION OF DV/V

[v,u]=butter(ordre,[DFc1 DFc2]*2/fe);
RESU=filtfilt(v,u,RESU);
figure(1)
imagesc([-
size(RESU,1)/2:size(RESU,1)/2]/fe,[1:size(RESU,2)]/24,RESU');drawnow
dv=zeros(1,size(RESU,2));
dv_sg8_21=dv;

smoothing
for l=1:size(RESU,1);
RESUs(l,[1:size(RESU,2)])=sgolayfilt(RESU(l,[1:size(RESU,2)]),1,lisse);
end
RESU=RESUs; figure; imagesc(RESU');

normalization
for i=1:size(RESU,2)
RESUn(:,i)=RESU(:,i)./max(abs(RESU(:,i)));
end
figure;
imagesc([-
size(RESU,1)/2:size(RESU,1)/2]/fe,[1:size(RESU,2)],RESUn');caxis([-1
1])
RESU=RESUn;
RESU(isnan(RESU))=0;
figure;hold on;

time=[-floor(size(RESU,1)/2):floor(size(RESU,1)/2)];
EPSILON=[-10e-2:1e-3:10e-2];
CC=zeros(length(EPSILON),size(RESU,2));
ref=nanmean(RESU(:,1:lasthour),2);
%%%%%%%%%%%%%%%
for t=1:1;
t
COMPUTING OF THE TIME WINDOW
[c index]=min(abs(time_corr-t1));
closestValue=time_corr(index)
leftvalueoftimewindow=find(time_corr==closestValue)
[c index]=min(abs(time_corr-t2));
closestValue=time_corr(index)
rightvalueoftimewindow=find(time_corr==closestValue)
time_window=[leftvalueoftimewindow:rightvalueoftimewindow];

EVALUATION OF dV/V
for jj=1:length(EPSILON)
time2=(time).*(1+EPSILON(jj));
ref2=interp1(time,ref,time2,'spline');%the interpolation of average cross
correlations
```

```
for hour=1:size(RESU,2)
temp=corrcoef(ref2(time_window),RESU(time_window,hour));
CC(jj,hour)=temp(2);%the matrix of cross correlations coefficients for
each
interpolated av. xcorr and filtered av, xcorr
end
end;
[cc b]=max(CC);
dv(t,:)=EPSILON(b)*100;
xt=find(cc>seuil);
lisse=3;
dv_sg8_21(t,:)=sgolayfilt(pchip(xt,EPSILON(b(find(cc>seuil)))*100,[1:size
(RESU,2)]),1,lisse);
drawnow
end


figure
imagesc([-size(RESU,1)/2:size(RESU,1)/2]/fe,[1:size(RESU,2)],RESU');
xlim([-1 1])
hold on
plot(dv_sg8_21./(100*EPSILON(end)),(1:size(RESU,2)),'w','markersize',4)
caxis([-1 1])
```

Appendix 3

Percentage of functioning days for each seismic station

Some stations had a battery's decay due to the low temperature reached during the winter. This results in missing data which lead to a discontinuity of the monitoring system. However, in order to overcome this problem, there are different solutions. First at all, where it is possible, such as in the study case, the seismic stations could be directly connected to the power grid. Otherwise, an alternative is the coupling of more powerful external batteries connected to bigger solar panels.

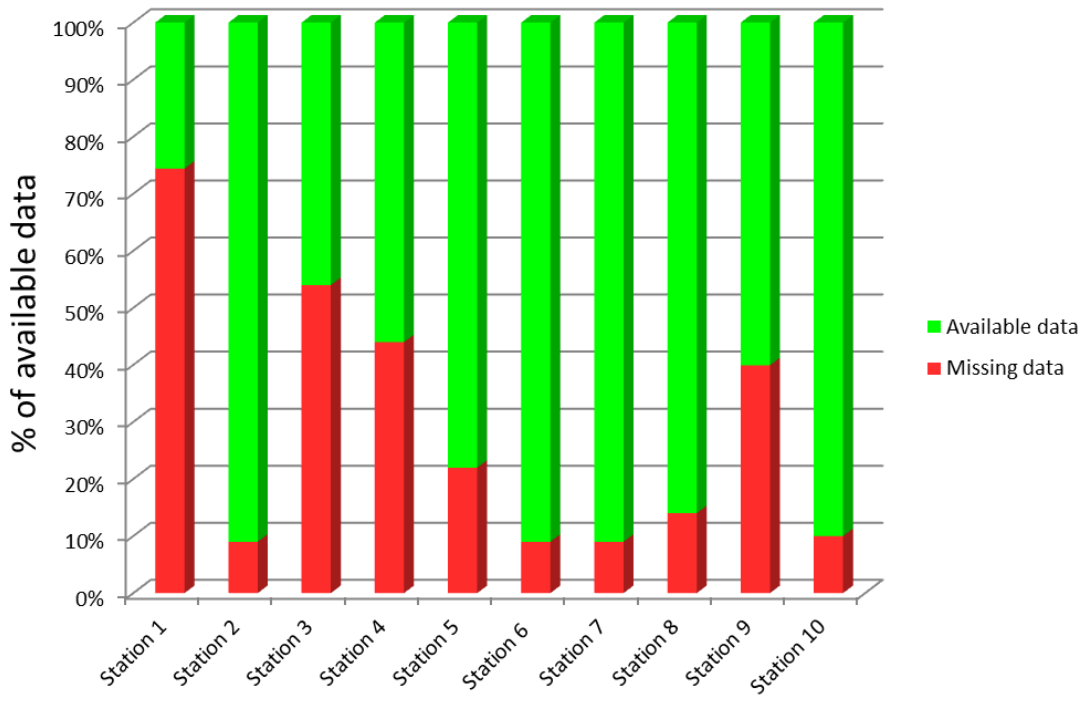

Graph 11. *Percentage of functioning days for each seismic station.*